UCL Université catholique de Louvain

École polytechnique de Louvain (EPL)

Augmented feedback for lower-limb amputees

Gait perturbation by vibrotactile stimulation of the patellar tendon: proof of concept

Dissertation presented by
Isabelle DE THYSEBAERT

for obtaining the Master's degree in
Biomedical Engineering

Supervisor(s)
Renaud RONSSE, Aleksandar JANKOVSKI

Reader(s)
Frédéric CRÈVECOEUR, Christine DETREMBLEUR

Academic year 2017-2018

Abstract

To contribute to research on augmented feedback for lower-limb amputees, I developed a gait perturbation experiment using inertial measurement units (IMUs) to obtain gait information in real time and activate a vibrotactile unit stimulating the patellar tendon. This thesis is a proof of concept of the use of IMU signals to activate a vibrotactile stimulation at a given time of the gait (heel-strike $\pm$ a delay). The shank angular velocity signal provided by the IMU is filtered and learned by adaptative oscillators to provide sufficiently strong detection conditions of foot-ground contact and the software and hardware delays are computed to be taken into account in the vibration activation. After a first experiment, the detection and activation conditions are re-examined and modified to overcome their weaknesses. The final real-time analysis of the signal comprises a 3Hz low-pass filter, a maxima detection based on 3 conditions and a step duration computation based on minima detection. The total delay between the real contact and the vibration of the unit is quantified and taken into account in the activation of the vibration.

Remerciements

Premièrement, je tiens à remercier mes promoteurs, le Professeur Renaud Ronsse et le Professeur Aleksandar Jankovski, pour leur encadrement et leurs conseils tout au long de la réalisation de ce mémoire.

Je tiens également à remercier le Professeur Christine Detrembleur, le Professeur André Mouraux, ainsi que leurs doctorants Laura Wallard et Baptiste Chemin pour le temps qu'ils ont consacré à l'élaboration du protocole expérimental ainsi que pour leurs conseils avisés dans leurs domaines respectifs d'analyse de la marche et de stimulation nerveuse.

Merci également au Professeur Frédéric Crèvecoeur d'avoir accepté d'être lecteur de ce mémoire.

Merci à Giulia Liberati pour sa disponibilité et le temps qu'elle a consacré à m'informer sur les unités vibrotactiles utilisées lors des expériences.

Un immense merci à Julien Lebleu sans qui l'utilisation et l'analyse des donneés IMU en temps réel n'aurait pas été possible. Merci pour ses conseils, pour le temps qu'il a consacré à la réalisation des expériences, ainsi que pour sa confiance.

Merci à Marie-Joy de Crombrugghe et Delphine De Tremerie d'avoir donné de leur temps pour mes expériences.

Finalement, un immense merci à mes parents et amis de m'avoir soutenue durant ces cinq années et, plus particulièrement, lors de la réalisation de ce mémoire. Merci de m'avoir remotivée lorsque j'en avais besoin et d'avoir cru en moi. Merci tout spécialement aux personnes qui ont accepté de relire ce mémoire.

La réalisation de ce mémoire n'aurait pas été possible sans toutes leurs contributions.

Isabelle de Thysebaert

Contents

Introduction

It is of common knowledge that patients who went through an amputation suffer from lack of sensory feedback from the amputated limb, among other medical conditions. For lower-limb amputees equipped with a prosthesis, this lack of sensory feedback induces an unnatural gait leading to additional medical conditions, either physical or psychological. The asymmetry of the gait [1, 2, 3, 4] resulting from the asymmetry of the sensory feedback is one of these conditions leading to many more such as poor balance [1, 5, 6, 7] and bad stability [8, 9]. Patients suffering from unnatural gait also have a high probability of undergoing muskuloskeletal diseases including osteoarthritis of the healthy leg, osteoporotic of the amputated leg or back pain [10, 1, 7, 11, 3, 4]. Finally, the cognitive effort needed to stand or walk will also increase [1] as well as the energy consumed during gait [12, 3, 4, 10, 9], which affects the psychological state of the patient.

Development of prosthesis with sensory feedback is expanding and, in parallel, lots of experiments are conducted to increase knowledge in this field. Among the external feedback modalities studied, we find mainly visual, auditory and tactile feedback, the latest comprising vibrotactile, electrotactile and mechanotactile stimulation. To contribute to research, the goal of this thesis is to develop a gait perturbation experiment consisting in a vibrotactile perturbation of the patellar tendon.

After a literature review describing a non exhaustive portion of the augmented feedback experiments already conducted, for upper and lower limb, as well as their results, the choice has been made to deliver the perturbation as a vibrotactile stimulation of the patellar tendon. In order to deliver this perturbation at a given gait phase, inertial measurement units were used to obtain a gait signal and analyse it in real time. The acquisition and treatment of the signal to recognise the gait phases as well as the quantification of the delays to take into account in the stimulation are described as a proof of concept of the experiment. The results of the first experiment are then exposed and the final experimental protocol is described after modification of the weak parts of the initial version. Finally, the expected results are exposed along with the tools to obtain them.

Chapter 1

Context

Before deciding which stimulation modality will be used during the experiment, it is important to remind the medical context behind the lack of feedback following an amputation. In addition, a complete state of the art is necessary to make an informed choice. This chapter will therefore expose the medical context in which this experiment stands then summarize the literature review on experiments studying sensory feedback.

1.1 Medical context

In order to understand the effects of sensory feedback lack on the gait of lower-limb amputees, the mechanisms involved in natural feedback are explained in this section. The successive phases of natural gait are then described and finally, the medical conditions induced by a lower-limb amputation are listed.

1.1.1 Natural feedback

The somatosensory system allows us to be aware of the current state of our body and of the surrounding environment at any time. The information about this state is transmitted by the activation of neuronal sensory receptors, producing a nerve impulse in the afferent nerve fibres. The stimulus is later translated and the modality, intensity, duration and localisation of the information are coded. The information can therefore be treated in the central nervous system (CNS).

The somatosensory system can be divided into four modalities for which the receptors, afferent fibres and location of treatment in the CNS differ. These modalities are the following [13]:

- Tactile sensitivity: mechanical stimulus on the body surface
- Proprioception: kinematics and dynamics of body parts (joint angles, muscle length, muscle tension...)
- Nociception: pain
- Thermal sensitivity

The first two modalities are part of the lemniscal system while the last two are part of the antero-lateral system. In the case of a prosthesis replacing a missing limb, the first two parts must be replaced in priority. Indeed, the second two are replaced by the physical limitations of the prosthesis. Therefore, we will only describe here the elements of the first two modalities.

Tactile sensitivity contains four receptor types (all encapsulated mechanoreceptors) responding to four different types of mechanical stimuli. These receptors are summarised in Table 1.1,

where adaptation is defined as a decrease of neuronal response for a constant stimulus.

		Adaptation of the afferent fibres	
		Slow	Fast
Receptor field	Small, superficial	Merkel disks Shape and texture	Meissner corpuscles Movement on the skin
	Large, deep	Ruffini corpuscles Pressure, cutaneous stretching	Pacinian corpuscles Vibrations

Table 1.1: Receptor types of tactile sensitivity.

Receptors for proprioception are divided into three categories corresponding to three different locations:

- Muscles: neuromuscular spindles.
  Free nerves ending in muscle axis, sensitive to muscle elongation. Two groups of afferent fibres, one coding for changes of muscle length and the second for constant muscle lengths.
- Tendons: Golgi tendons organs.
  Sensitive to stress changes in tendons.
- Articulations: close to Ruffini and Pacinian corpuscles.
  Fingers movement mainly [9] .

1.1.2 Natural gait

During gait, both legs go through the same succession of eight steps. In natural gait, and for healthy people, each step has the same duration for both legs. These steps are listed below and illustrated in Figure 1.1.

1. Initial contact: heel-ground contact, also called heel-strike.
2. Loading response: first half of the foot (heel-mid) in contact with the ground.
3. Mid stance: entire foot-ground contact, displacement of the gravity center.
4. Terminal stance: second half of the foot (mid-toe) in contact with the ground.
5. Pre swing: toe-ground contact, also called toe-off.
6. Initial swing: foot take-off.
7. Mid swing: no foot-ground contact.
8. Terminal swing: preparation for initial contact.

In the control of lower limbs, and more precisely during gait, one of the main information needed to compute the motor command is the center of pressure (CoP), measured by mechanoreceptors in the insole. Indeed, the actual phase of the gait cycle can be directly derived from its position in the heel-to-toe movement [8]. But feedback from other modalities mentioned above also plays an important role in gait kinematics [9].

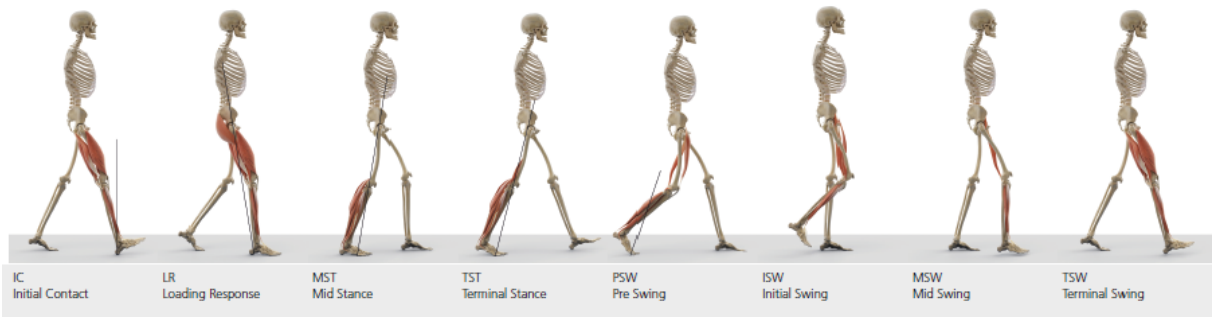

Figure 1.1: Phases of the gait cycle [14].

1.1.3 Medical conditions induced by an amputation

When a limb is amputated, it loses a part of the muscles activated during the limb movements as well as the neuronal receptors detecting the state of the limb and its environment and the nerves relaying this information. Even with a prosthesis using an activation system close to natural muscles, the lack of sensory information prevents the brain to correctly compute the motor command for the residual muscles playing a role in the global movement. Indeed, the closed loop is not complete anymore and, therefore, the internal model can not be updated. The new state of the limb is thus not taken into account while computing motor commands and the actual movement will not correspond to the movement predicted by the internal model [15].

After a lower limb amputation, the phase in the gait cycle cannot be precisely estimated without CoP feedback, and the information transmitted by the contact with the prosthesis is not enough to derive it either [8]. The state of the limb is thus not known by the patient [16]. Patient walking with prosthesis lacking sufficient feedback will thus undergo important drawbacks in their gait. It is important to note that some of these problems are not only due to the lack of sensory feedback but also to motor deficiency.

Among these drawbacks, the gait pattern will show an increased stance phase on the healthy limb and a decreased one on the prosthesis side [10, 1, 5, 6, 7], resulting in a shorter stride length of the healthy limb [5, 6]. The gait kinematics will thus show asymmetries [1, 2, 3, 4], the weight will be unequally distributed [10] and the trunk sway will be more important [7]. This condition will lead to a poor balance [1, 5, 6, 7] and a bad stability [8, 9].
Moreover, lower-limb amputees have a high probability of undergoing muskuloskeletal diseases such as osteoarthritis of the healthy leg, osteoporotic of the amputated leg or back pain [10, 1, 7, 11, 3, 4].
The cognitive effort needed to stand or walk will also increase [1] as well as the energy consumed during gait [12, 3, 4, 10, 9]. It is also important to mention that the fine sensations needed to discriminate the features of an object will be lost too [17], even though this loss is rather related to upper-limb amputation.

1.2 State of the art

When a lost limb is replaced by a prosthesis, sensory feedback giving information about the state of the prosthesis and its surrounding environment is not naturally available. To avoid going through the non exhaustive list of drawbacks given above, an artificial sensory feedback can be given to the patient. This feedback can be given via sensory augmentation or sensory substitution. Since augmentation consist in giving complementary information to an attenuated feedback, we need to focus on sensory substitution. Indeed, in the case of an amputation, the feedback from the limb is entirely lost, not only attenuated. The purpose of sensory substitution is to replace a lost feedback, either by using a different sensory channel, or by using the same with a different modality [18, 19, 9, 15].
The existing modalities can be divided in two main categories : non-invasive and invasive feedback. The first category includes visual, auditory and different modalities of tactile feedback and the second category comprises mainly direct neural stimulation, using implanted electrodes to transmit the sensory information directly to the peripheral nervous system [18, 19, 9].

Besides the modality, the information to be transmitted must also be chosen carefully since too much information induce a too important cognitive load for the user [9].
For the tactile modalities, targeted sensory reinnervation can be applied previously to approach the sensation to the natural one. This surgery consist in reinnervating sensory nerves previously driving back sensory information from the amputated limb in order to create a map on a practical skin area where the feedback channel elements will be placed [18, 19].

Table 1.2 and the following subsections summarize a non exhaustive list of articles proposing sensory feedback solutions for lower limb and upper limb prostheses.

Table 1.2: Summary of the feedback methods, recorded signals and results obtained in the articles presented in the state of the art.

Articles	Feedback method	Signal recorded	Results
Bamberg et al.[10]	**Auditory** : Gait asymmetry > threshold	LEAFS : 12 force resistors	LEAFS ok
Buma et al.[20]	**Electrotactile** : 3 to 8 electrodes knee angle spatially mapped	/	Adaptation = 15min reduced by intermittent stimulation
Canino and Fite[16]	**Vibrotactile** : 3 vibrators - **Mechanotactile** : 3 units region of sinusoidal trajectory or error direction	/	Performances improved
Canino and Fite[21]	**Vibrotactile** : 3 vibrators - **Mechanotactile** : 3 units error direction	2 pressure sensors under foot	Performances improved
Chow and Cheng[11]	**Auditory** : Load > threshold	load-monitoring device	Less overload
Crea et al.[1]	**Vibrotactile** : 3 vibrators gait phase transition	64 pressure sensors under foot	Effect of stimulation delay
D'Alonzo et al.[22]	**Hybrid = Vibrotactile + Electrotactile** : 9 combinations	/	Discrimination improved
D'Alonzo et al.[23]	**Hybrid = Vibrotactile + Electrotactile** : 5 channels	1 pressure sensors/finger	Discrimination improved
Dosen et al.[24]	**Visual** : Screen EMG values and grasping force	EMG and force sensors on fingers	Performances improved with EMG
Dosen et al.[25]	**Electrotactile** : 16 electrodes Spatial (and frequency) mapping	Force sensors on fingers	Better discrimination of spatial AND frequency
Fan et al.[12]	**Mechanotactile** : 4 units pressure magnitude and direction	4 force sensors under foot	Good discrimination
Jorgovanovic et al.[26]	**Electrotactile** : 2 electrodes	Grasping force	Performances improved
Lee, Lin and Soon[5, 6]	**Visual** : Screen, pressure distribution **Auditory** : 1 level/force range	2 force sensors under foot	Performances improved
Oddo et al.[17]	**Invasive** : 1 needle or electrode gratings = spike trains	4 piezoresistors on fingertips	Good discrimination
Ortiz-Catalan et al.[27]	**Invasive** : 1 unit	/	Sensation reproducibility
Plauché et al.[8]	**Vibrotactile** : 8 vibrators CoP location or error direction	16 force sensors under foot	Performances improved error direction better
Raspopovic et al.[28]	**Invasive** : 4 electrodes	Force sensors on thumb, index, little finger	Performances improved
Redd and Bamberg[2]	**Visual** : Smartphone, gait symmetry ratio **Auditory** : Alarm, too much time on one limb **Vibrotactile** : Smartphone, too much time on one limb	2 pressure sensors under foot	/ Not practical according to subjects
Webb et al.[3, 4]	**Electrotactile** : 8 electrodes	/	Good discrimination
Wendelken et al.[29]	**Invasive** : 100 micro-electrodes	Touch sensation on hand palm	Good discrimination, various sensations
Wentink et al.[30]	**Vibrotactile** : 8 vibrators sequential or simultaneous	/	Sequential > simultaneous
Yang et al.[7]	**Auditory** : symmetry ratio > threshold	Force sensors under foot	Performances improved
Zambarbieri et al.[15]	**Vibrotactile** : 2 or 4 vibrators spatial mapping	2 or 4 force sensors under foot	Positive feeling

1.2.1 Non-invasive

Lower limb

Three feedback modalities have been mainly studied to transmit lower limb information: visual, auditory and tactile feedback. While the first two are hardly unobtrusive, tactile feedback is portable and can be delivered in three different ways : through vibrations, electrodes or mechanical deformations.

Visual feedback

Visual feedback can be given in different ways, but only a few of them are portable. It is provided on a screen in most of the tests but can also be projected on the ground, given via a smartphone or through virtual reality. The advantage of this technique is that it has been widely tested with good results and its main drawback is the risk of overloading the visual path [9].

In their articles, **Lee, Lin and Soon**[5, 6] proposed a visual feedback displayed on a screen. This feedback consist in a representation of the pressure distribution under the foot for which the intensity at each location is given by a colour. An auditory feedback is provided in parallel (explained in the next section). Together, the feedbacks allow the subject to have information about their gait pattern and the level of weight carried by their prosthesis. The information provided is derived from the measures of the heel-strike and the toe-off taken by two force sensing resistors under the foot. The results were obtained by comparing different parameters of the gait pattern with and without feedback. With visual feedback, the stance time in the prosthetic side increases while the one in the healthy limb decreases thus the stance phase and swing phase are closer in duration. The number of steps per minutes also increases. The gait with feedback is thus more symmetrical and closer to the natural gait. **Redd and Bamberg**[2] proposed a portable device by providing visual feedback on a smartphone (offering a choice of one or more between visual, auditory and vibrotactile feedback). The visual feedback consist in a graph displaying the gait symmetry ratio $\frac{\text{Left stance time}}{\text{Right stance time}}$. The optimal ratio ($= 1$) is chosen as the center and a deviation of the ratio from this optimal value is represented by a visual deviation from the origin (a deviation to the left when the stance time on the left foot is too important and vice versa). The information provided is derived from the measures of heel-strike and toe-off taken by 2x2 pressure sensors under the feet.

Visual feedback is recognized for giving good results. Indeed, **Canino and Fite**[16][21], among others, used it as a control condition in the validation of their feedback system. They used vibrotactile and mechanical feedback to deliver the pattern of a movement to follow or an indication of the correction to make when the difference between the pattern and the actual movement was too important. In this case, the visual feedback during the control condition gave an overlay of the desired and actual trajectory. Visual feedback is often used as a control condition, meaning that its efficacy is accepted. Indeed, compared to tactile feedback, it gives a more continuous and more precise information leading to less uncertainties [25]. Furthermore, it is important to note that patients tend to be more frustrated when they make a mistake with visual feedback than with tactile feedback [16].

Auditory feedback

Auditory feedback can be transmitted via speakers or with headphones to be used in everyday life. The ways to make the information vary are numerous : intensity, volume, timbre or stereo balance. The advantages and drawbacks are the same as for visual feedback [9].

Chow and Cheng[11] proposed as auditory feedback an alarm sounding when the amount of load supported by the prosthesis reach a given threshold. The amount of load was measured

right below the prosthesis socket by a load monitoring device. To assess the device performance, the load-time curves were averaged over all the gait cycles at every session. The results showed that the mean peak was lower with feedback than without, and never exceeded the threshold, and that the variance from step to step decreased when the feedback was given. The results obtained by **Lee, Lin and Soon**[5, 6] with their feedback combining visual and auditory channels were explained in the previous subsection. To obtain those results, an indication about the force range measured by the sensors was given through two loudspeakers with three volume levels corresponding to three ranges. The subjects reported that the auditory feedback was more comfortable than the visual feedback. The solution given by **Redd and Bamberg**[2] in the previous subsection also proposed an auditory feedback. Based on the same measurements, this feedback was given in the form of an alarm sounding one time if the subject stayed too much time on its left limb and two times if he stayed too much time on its right limb. The time-limit was given by a pre-set threshold. The main disadvantage of this solution according to the subjects was the difficulty to remember this threshold thus to correct the error when the alarm sounded. The auditory feedback proposed by **Yang et al.**[7] is similar to the previous one since the alarm here was a loud beep sounding when the symmetry ratio (defined here as $\frac{\text{Stance time affected}}{\text{Stance time healthy}}$) dropped under a defined threshold. The stance time was calculated from the measures given by 10 force-sensitive resistors under the feet. This feedback method has been tested on three subjects and an improvement of the symmetry ratio as well as a decrease of the trunk sway were noticed in two of them. In 2010, **Bamberg et al.**[10] tested the accuracy of a new measuring system to quantify gait asymmetries in order to provide a auditory feedback when the latter is above a given threshold. This system, called Lower Extremity Ambulation Feedback System (LEAFS) was composed of 12 force sensing resistors under the foot; 4 under the heel, 2 under the great toe and 6 under the heads of the metatarsalphalangeal joints. Heel-strike and toe-off were identified with those measures and the gait asymmetry could be derived. To validate the LEAFS measuring system, the data obtained were compared to the ones obtained by 10 cameras detecting feet movements through markers placed on toe and heel of both feet, and 4 force plates used as references on the path. By comparing the asymmetry detections of both systems, we saw that the asymmetry detection was nearly the same and that the stance time of the healthy limb was, as expected, longer than that of the prosthetic limb. The possible improvements of the LEAFS measuring system were decreasing the sampling frequency (currently at 150Hz) or increasing the number of sensors in the sole.

Tactile feedback

Tactile feedback includes three main categories: vibrotactile, electrotactile and mechanical deformation. For each of them, the information can be transmitted to the patient at different locations and with different patterns but is of low dimension, even though combination of those modalities have been tested to increase the amount of information provided [22, 23]. The location on the body where the information is transmitted has an important impact on the discrimination capability since the receptors density is not constant [19, 9]. The adaptation is also an important parameter to take into account since it reduces the neuronal response thus the tactile sensation of the feedback.

Vibrotactile feedback is applied via vibrating element on the skin with varying amplitude and/or frequency of vibration, with a frequency between 10 and 500Hz. Other features like pulse duration or shape can also be modulated [18, 19]. Vibrotactile feedback is the modality the most subject to adaptation, especially during continuous stimulation.

As explained in the lasts subsections, **Redd and Bamberg**[2] tested a feedback provided by smartphone. The vibrotactile feedback consisted in two types of vibrating pulses depending on the correction to make. A small pulse indicated a too long stance phase of the left side while

a longer pulse stood for a too long right stance phase. As in the auditory feedback, the main difficulty of use of this system was the difficulty to remember the threshold. This way to provide a vibrotactile feedback is not usual since, in most of the cases, this feedback is provided through rotating motors in direct contact with the skin. In 2001, **Zambarbieri et al.**[15] proposed a solution in which 2 or 4 vibrators placed on the anterior and posterior side of the thigh provided the force measured by 2 or 4 force-sensitive resistors under the foot. The first feeling given by the subjects were a good acceptance and a sense of assistance in the rehabilitation process.

In 2011, **Wentink et al.**[30] performed tests with 8 vibrators placed over the thigh circumference to analyse the effect of different parameters of vibrotactile stimulation such as its frequency and the spacial and temporal characteristics of stimulation. For their first test, the vibrators were placed by pair; one medially, one laterally, one posterior and one anterior. Each pair was stimulated at a time with frequencies between 30 and 80Hz. As a result, the observation was made that the felt intensity increased with frequency, especially on the posterior and medial side where it was poor between 30 and 50Hz, increased rapidly between 50 and 70Hz and showed a saturation between 70 and 80Hz. For the second test, the 8 vibrators were placed in a row, 2cm apart from their neighbours. The frequency of stimulation was set at 80Hz and the vibrators were activated sequentially or simultaneously by 1, 2 or 3. The subjects were asked how many vibrators had been activated and where. Resulting from this second test, sequential stimulation showed a better detection rate. The number of stimuli was indeed more often correct. The last test was an adaptation test and one element was activated at 80Hz during 15min. As a result, half of the subjects did not feel anything after 15 minutes and more than half of them noticed a decrease of sensation due to adaptation.

In 2015, **Crea et al.**[1] proposed a feedback system composed of 3 miniaturized vibrating elements. Since the targeted patients were above-knee amputees, those vibrators were placed on the front, external and back sides of the thigh, more precisely on the muscles bellies. The purpose was to activate Pacinian corpuscles and the frequency was therefore set at 230Hz. The elements were activated during gait phase transitions in order to avoid adaptation. Those three phases, each corresponding to the vibration of one element, were toe-off (front side), flat foot (lateral side) and heel-strike (back side). To do so, the vertical ground reaction and the coordinates of the CoP were derived from 64 pressure-sensitive elements under each foot. The gait was then divided in three phases : the first half of the stance (from heel to half), the second half of the stance (from half to toe) and the swing phase. The gait phase transitions could thus be easily detected. The tests of the system were mainly focused on the perception of stimulation during walk by analysing the detection of errors or delays in the feedback. As results, vibrations of the front and lateral elements were less correctly detected as the delay between the phase and the vibration increase while the detection rate of the vibration of the back side element increased. The detection of a wrong vibration however was constant across all vibrators. Finally, the stance duration, swing duration and step cadence were not significantly different when a feedback was given with delay, on the wrong vibrator or missing, meaning that no gait asymmetry was induced in able-bodies subjects.

In 2016, **Canino and Fite**[16] tested a vibrotactile feedback system comprising 3 vibrating motors in a line vibrating at 250Hz, the ideal frequency to activate Pacinian corpuscles. During the test, the subjects had to follow given periodic trajectories and were guided by the vibrotactile feedback. Each element corresponded to one part of the sinusoid in a logical order of stimulation (vibrator 1 for the low region, 2 for the mean region and 3 for the peak region) and each trajectory corresponded to a pattern of 5 actuations ($1 \rightarrow 2 \rightarrow 3 \rightarrow 2 \rightarrow 1$ for example). If the actual trajectory did not correspond anymore to the desired one, the system transitioned to corrective feedback. In this case, the activation pattern became $3 \rightarrow 2 \rightarrow 1$ or $1 \rightarrow 2 \rightarrow 3$ in function of the needed correction (flexion or extension). The results of the tests showed that the trajectories were less variable and closer to the desired trajectory with feedback than without. In a second

article [21], they used the same conditions of stimulation but, this time, subjects had to stabilize their limb around a given angle. In this case, the more proximal element was stimulated if an extension was needed to approach the angle, the middle element when the subject was close to the given angle, and the distal element when a flexion was needed. As a result, the limb angle was closer to the trajectory with feedback than without. Attention must be given in the critique of this system since one subject underwent desensitization during the test.

The system proposed by **Plauché et al.**[8] used 8 vibrators equally spaced around the thigh, vibrating at a frequency of 250Hz to activate Pacinian corpuscles. The information send as feedback was derived from 16 force-sensing resistors placed under the main pressure point of the foot to measure the CoP. The first feedback system tested was constantly activated since it gave a geographical mapping of the CoP; the vibrators were activated from back to front when the CoP moved from heel to toe. The second test used a corrective feedback. The element vibrated when the CoP derived of more than 1cm from its normal path in the vibrator direction. This second system allowed a non-continuous stimulation thus decreased the risk of adaptation. In both systems, the variance of stride length and step width was reduced compared with a situation without feedback. Mainly in the corrective system, the variability of the trunk sway decreased, but improvements were also noticed in the constant system. In general, more subjects showed improvements with the corrective than with the constant system.

Electrotactile feedback is applied by the use of electrodes providing a local waveform current varying in amplitude (1-20mA), shape (with a biphasic phase described as more comfortable), frequency (1Hz-5kHz) and/or duration. Its advantages are a fast response an a low power consumption [19]. The stimulation is sensed as a vibration when delivered with a low pulse rate and as a constant pressure when the pulse rate is higher [22].

In 2007, **Buma et al.**[20] wrote an article in which they tested several parameters of their feedback method. The latter consisted in 3 to 8 electrodes spatially mapping the knee angle of a prosthesis during gait, each electrode corresponding to one part of the angular range. This system was placed on the medial side of the thigh, with electrodes current-controlled and a pulse frequency fixed to 30Hz. The tests described in the articles have been performed in order to fix some parameters to avoid adaptation. The first test consisted in a continuous stimulation at three current levels set to 20%, 50% and 80% of the range [sensation threshold; pain threshold]. The sensation was described by the subjects through a Visual Analogue Scale (VAS) every 40s. The comparison of the sensations felt at 900s showed that the sensation level was null for the stimulations at 20% and 50% but not for the stimulation at 80%. The sensation level decreases thus more slowly for higher stimulation currents. Moreover, the results confirmed that adaptation happens within 15 minutes. During the second experiment, the stimulation was delivered through different intermittent patterns varying in burst duration and interval. In this case, the current amplitude was set to 80%. This experiment showed that adaptation is reduced when using intermittent patterns rather than continuous stimulation, especially when interbursts last more than 0.3s. The number of electrodes in the proposed solution should thus be large enough to satisfy this condition and the solution should foresee an intermittent stimulation system for static situations like standing. Finally, the sensation and pain thresholds were determined before and after each experiment. The sensation threshold showed a significant difference between the two measures in both experiments, with an increasing value, while the change in pain threshold was significant only for the first experiment.

In articles written in 2011 and 2012, **Webb et al.**[3, 4] described a system composed of 8 electrodes placed around the stump. Several features of the system were tested in order to develop a system for which the location and intensity of the activated electrode give respectively the error direction and magnitude. The different tests were performed on subjects in different positions among laying supine, performing a static knee flexion when standing or a static knee

extension when seated, and on walking subjects. The first test consisted in determining the sensation and pain thresholds for each electrode, by stimulating at 40Hz, 60Hz and 80Hz with increasing intensity. The results showed that the difference between the two thresholds was smaller for higher frequencies. The second test consisted in randomly stimulating electrodes at 40Hz, 60Hz and 80Hz with an intensity defined as the mean of the two thresholds. The locations of the activated electrodes were detected with a detection rate of 98%. Finally, for the third test, the stimulus moved around the thigh in clockwise or anticlockwise direction and with low, medium or fast velocity. In this case, the detection rate of the direction and velocity of the stimulus was equal to 100%. A more general result in this study was a discomfort felt by most of the subjects for every stimulation intensities at 80Hz.

Mechanotactile (or mechanical deformation) stimulation is applied by a force normal to the skin. Accuracy, precision, range, resolution and bandwidth are the parameters that can be varied in this modality. Mechanotactile stimulation is less used than vibrotactile or electrotactile stimulations since such sensations can be elicited through vibrations on the skin [18, 19].

In 2008, **Fan et al.**[12] proposed a system composed of four pneumatically controlled balloons placed on the anterior, posterior, medial and lateral sides of the residual limb. Each balloon corresponded to one of the four force sensors placed under the foot. The force levels were measured in a discrete way and so were the pressure levels delivered. In a first test, subjects had to detect the one inflated balloon or the sequence of three inflated balloons while the balloons could have two states: not inflated or fully inflated. The identification rate was 99%. In the second test, subjects had to give the sequence of directions in a test where the balloons were used as navigation guide: anterior balloon activated for forward direction, posterior for backward, medial and lateral for left and right (in function of the amputated leg). The directions indicated could also be oblique with combination of stimulations. In this test, the rate of accuracy was 94.8%. In the third test, three inflation levels were used (0, 40 and 100% of the maximum level) and a balloon was sequentially actuated with two different levels. In 92.6% of the cases, the subjects could tell which inflation was larger. Finally, the complete system was tested and subjects had to give the sequence of actuation. In this case, 95.8% of the sequences were correctly identified.

In 2016, during the validation tests of their vibrotactile stimulus method explained sooner, **Canino and Fite**[16][21] tested two other feedback systems based on mechanical deformation. The first system[16] was pneumatically actuated and delivered quasi-static pressure stimulus, ideal to activate Merkel disks, with 3 pressure vessels. As a reminder, the tests consisted in following periodic trajectories while receiving clues about the actual phase of the sinusoid through the feedback interface. The feedback switched to corrective mode if the actual trajectory went too far from the desired one. While both feedback systems (vibrotactile and mechanotactile) improved the performances of the subjects, mechanotactile stimulation still showed better results than vibrotactile when combined to visual feedback. In the second system[21], three aluminium pressure vessels pneumatically actuated and placed in an array were used to deliver the feedback in order to stimulate Merkel disks. As for the vibrotactile elements, each pressure vessel was used to orient the subjects in one direction (extension or flexion needed) to help them reach the right angle. In this case again,the mechanical deformation system showed better results than vibrotactile stimulation.

The table 1.3 summarizes the results of the experiments on lower limb described hereabove. All modalities induced positive results, even though visual and auditory feedback are generally not portable thus not applicable in daily life. Regarding tactile feedback, the bigger drawback highlighted was adaptation, but it can be reduced by fixing properly the stimulation parameters or by choosing a discrete feedback over a continuous one.

Articles	Results
Visual feedback	
Lee, Lin and Soon[5, 6]	More symmetrical gait
Redd and Bamberg[2]	Feedback not practical
Canino and Fite[16]	More frustration when mistake
Canino and Fite[21]	Control condition
Auditory feedback	
Chow and Cheng[11]	Less load on prosthesis
Lee, Lin and Soon[5, 6]	More comfortable than visual
Redd and Bamberg[2]	Threshold difficult to remember
Yang et al.[7]	More symmetrical gait, less trunk sway
Bamberg et al.[10]	Good detection of asymmetries
Vibrotactile feedback	
Redd and Bamberg[2]	Threshold difficult to remember
Zambarbieri et al.[15]	Good acceptance
Wentink et al.[30]	Better detection rate of sequential stimulation
Crea et al.[1]	Delay of stimulation has no effect on results
Canino and Fite[16]	Less variables trajectories, closer to target
Canino and Fite[21]	Angle closer to trajectory
Plauché et al.[8]	Improvements in both systems, bigger one in corrective
Electrotactile feedback	
Buma et al.[20]	Adaptation faster for continuous stimulation
Webb et al.[3, 4]	Good detection of the stimulus in all tests
Mechanotactile feedback	
Fan et al.[12]	Good detection of the stimulus in all tests
Canino and Fite[16]	Better results than vibrotactile
Canino and Fite[21]	Better results than vibrotactile

Table 1.3: Summary of the results for lower limb feedback.

Upper limb

Upper limb prostheses need a more complex feedback system to mimic at best the natural sensory feedback of upper limbs. Indeed, finger movements are more complex and need to be more precise than lower limb movements, and tactile information transmitted by hands and fingers is also more complete, resulting in a more important rate of neural receptors, thus a larger information. Therefore, it is interesting to summarize some articles testing upper limb prostheses feedback systems delivering more complex information than lower limb prostheses.

Visual feedback

In 2015, **Dosen et al.**[24] used visual feedback to compare two feedbacks in order to implement the most efficient one as tactile feedback. The upper-limb prosthesis was myoelectrically controlled and its virtual representation on a screen was used to provide an optimal view of the prosthesis to the subject. Position and fore sensors were used to reconstruct the virtual prosthesis and to measure the grasping force that is part of the feedback signal in both cases. In the second case, a copy of the EMG controlling the prosthesis was added to the feedback signal to give an indication of the muscle activity to the subject. The visual feedback was given on a screen. Additionally to the ideal vision of the prosthesis were a horizontal bar giving the generated and targeted grasping force and, in the second feedback case, a horizontal bar giving the value of the measured myoelectric signals of the flexor and extensor muscles. The differences between the two feedback signals were assessed through two tests : routine grasping and force steering. Routine grasping consisted in reaching the corresponding grasping force (among 30%, 50% and 70% of the maximal force of the prosthesis) directly after the contact with the target and force steering consisted in following a path of target forces. In the routine grasping test, results showed less variable forces across trials and force levels when the EMG was provided additionally to the grasping force. Moreover, it took several trials without EMG feedback to reach the desired force when set to 50% and 70%. In the force steering trial, the forces increased and decreased in steps in both cases but with smaller steps and a force profile closer to the desired force path when EMG was provided. Without EMG, the variation around the reference trajectory was more important and presented larger overshoots, with several drops to zero. The performances in both tests were thus improved by the addition of EMG feedback to the grasping force feedback.

As for lower-limb prostheses, visual feedback is also used as a control condition for upper-limb prostheses. Indeed, **Dosen et al.**[25] used it as a control condition in the validation of their feedback system. **Dosen et al.** used an electrotactile feedback in a grasping test (in upper limb prosthesis) and replaced the prosthesis by a visual representation in order to give a clear vision of its movements to the patient. For the control condition, the grasping force was also provided on a screen in the form of a vertical bar. **D'Alonzo et al.**[22, 23] and **Jorgovanovic et al.**[26] also used visual feedback in a learning process before testing their devices. **D'Alonzo et al.** showed the activated electrode or vibrator when a sensation was felt by the subject to help him associate the sensation to its space location and **Jorgovanovic et al.** projected a bar graph of the grasping force (in upper limb prosthesis) next to the representation of the prosthesis (used during all the tests, as in [25]) for the subject to associate a value to the sensed grasping force.

Electrotactile feedback

In 2014, **Jorgovanovic et al.**[26] proposed a feedback system for upper limb prosthesis consisting in two concentric electrodes placed on the dorsal side of the forearm. The two electrodes gave the same information but their combination allowed a better quality of information, facilitating the discrimination of the sensation. The feedback to deliver was the grasping force, given here by the inclination of a joystick controlling a virtual prosthesis. This inclination was proportional to the hand closing speed in first place, then to the rate of growth of the grasping force. The pulses were delivered with a frequency of 100Hz in order to give an impression of

constant pressure and were modulated by their width. Subjects had to lift objects characterised by a minimum force to avoid slipping and a maximum force to avoid breaking. Once the grasping force was in between, a pushbutton was used to indicate the start of the lifting phase. After three training phases with additional visual feedback to familiarize subjects with the system, the latter was validated in 5 phases. During the first two phases, the same objects as in the training phases were presented, first with then without electrotactile feedback. During the second two phases, the same objects were presented with a doubled force response of the joystick, first without then with electrotactile feedback. During the last phase, the object presented were derived from the known objects (combined, scaled, or objects of similar weights). Along all the trials, the results were the following : the success rate was 70% when feedback was provided while only 15-20% without feedback. The grasping force in failed trials was closer to the targeted force range when feedback was provided and the correction after a failed trial was also better in trials with feedback than without. The time to complete the task was also different in both cases. Indeed, subjects paid more attention to the control when feedback was provided and therefore took more time. The inclination of the joystick was indeed more constant in cases without feedback, meaning subjects modulated less the rate of increase. A difference of modulation was also seen between smaller and heavier objects, especially in feedback cases. The control was finer, with more steps for small and medium objects and was coarser for heavier ones. Finally, the adaptation from known to unknown objects in the last phase showed good results for light objects but not for heavier ones.

In 2017, **Dosen et al.**[25] also proposed an electrotactile feedback system for upper limb prosthesis. This system was composed of 16 electrodes placed around the forearm and providing information about the grasping force measured by sensors on the prosthesis. Information was provided either using only spacial modulation (SPA) or using spacial and frequency modulation (MIX). In the first case (SPA), the force range was divided in 15 with each electrode corresponding to one subrange (with increasing value moving in one direction around the circumference). In this case, subjects only needed to discriminate the location. In the second case (MIX), the subranges were coded by activation of a certain group of 2 to 5 electrodes at a certain frequency (among 3). In this case, subjects still needed to discriminate the location, but less precisely, and needed to discriminate the frequency in addition. As a control condition, a visual feedback was given by providing the grasping force on a bar graph (VIS). The validation was made in three phases after a training phase with additional verbal feedback. Each phase was performed with SPA, MIX and VIS feedback. During the first phase, subjects had to recognize the force range from the stimulation. The results showed a better discrimination of the stimuli in MIX than in SPA. Errors in frequencies in MIX were generally located to the neighbouring frequencies and errors in location in SPA located in the neighbouring electrodes. The second phase was a grasping task during which subjects had to grip an object with a force as close as possible to the desired one, fixed at 30%, 50% or 70% of the maximum. The results were similar in the three situations: the variability was located around targeted levels with more variability for higher levels (one level above or below for low force levels and up to four levels of error for higher force levels). The last phase was a force tracking task. Subjects had to modulate the grasping force to follow a trajectory visually given. The results showed a better tracking with visual feedback but still abrupt changes of grasping force in all cases. In general, the performances were thus similar in both modulation methods even if the discrimination seemed easier in MIX modulation. It also showed by comparison with visual feedback that electrotactile feedback can lead to the same performances.

Hybrid feedback

In the articles written by **D'Alonzo et al.**[22][23] in 2013 and 2014, hybrid solutions combining vibrotactile and electotactile stimulation are presented and compared to vibrotactile and electrotactile stimulation.

In the first article[22], the purpose was to analyse hybrid feedback as a solution for multi-

information feedback. 3 vibratory elements were placed on top of each other and on top of the inner part of a concentric electrode. This system was placed on the anterior side of the mid forearm. Pretest consisted in determining for which frequency of the electrical stimulation was it easier for the subjects to discriminate vibrotactile and electrotactile stimulus. Indeed, a low pulse rate induces a vibration sensation while a higher pulse rate induces a constant pressure sensation. Since the intensity of the induced vibrations was set higher than the intensity of the electrical stimulus, there was a chance that the second would be masked by the first. For this pretest, the frequency of vibration was 160Hz, and the two tested pulse rate of electrical stimulation were 25Hz and 100Hz. To test the discrimination ability, subjects had to classify three levels of intensities provided in sequences of two, at 25Hz and 100Hz, and simultaneously with vibrotactile stimulation. The outcome showed a higher recognition rate at a vibration frequency of 100Hz. During the validation tests, 6 feedback systems were compared to assess the performance of the hybrid system. The first system, HyVE9, provided 9 combinations of vibrotactile and electrotactile stimulus, each of them with 3 intensities levels. The second system, HyVE9z, provided the same 9 combinations except that the medium intensity of vibrotactile stimulation was set to no stimulation. ELE3 and VIB3 provided the same 3 intensity levels as HyVE9 but for one modality at a time, and ELE9 and VIB9 provided 9 intensity levels for one modality at a time. First, the comparison of the hybrid systems with ELE3 and VIB3 showed that the ability to detect and recognize a stimulus in one modality was not affected by the presence of the other modality neither by its intensity. Indeed, the marginal recognition rates and the recognition rate in ELE3 and VIB3 were similar. Secondly, the comparison of the hybrid systems with single modalities systems of 9 intensities showed that hybrid systems have higher recognition rate. Indeed, in single modality, the recognition rate decreases when the number of levels increases. Hybrid systems are thus more efficient since it comprises less levels for each modality but still deliver the same amount of information. Finally, the comparison of the two hybrid systems showed a better recognition rate in HyVE9z than HyVE9. Indeed, the marginal recognition rate for vibrotactile is higher, but the recognition rate of electrotactile is not affected.

In the second article[23], the purpose was to have a 5 channel interface in order to have a correspondence for each sensor if we use one touch sensor per finger. The interface was placed at mid forearm and was composed of three electrodes in a line with two vibrators superposing the two external electrodes. In the hybrid solution (HyVE4) tested and compared to single-modality interfaces, the distance between the centres of the electrodes was 4cm. Two single-modality interfaces of same center-to-center distance (4cm) and larger total length were compared to the hybrid solution : ELE4, composed of 5 electrodes, and VIB4, composed of 5 vibrators. One single-modality interface of same total length and smaller center-to-center distance (2cm) composed of 5 vibrators, VIB2, was also compared to the hybrid solution. For all solutions, the electrodes stimulated at 100Hz to feel like a constant pressure and the vibrators stimulated at 120Hz. The comparison between the four solutions was made through two tests : recognition of a single stimulus and recognition of a pattern of stimuli. The results shown by the first test were a similar, or better recognition rate of HyVE4 compared to ELE4 and VIB4 and a significantly lower recognition rate of ELE2. During the second test, the general number of misrecognitions increased slightly and the recognition rate of ELE2 was still lower, with more misrecognitions medially than laterally. In both tests, the recognition rate was thus higher or comparable in the hybrid solutions compared to single-modality solutions of same center-to-center distance and was higher compared to single-modality solutions of same-size but smaller center-to-center distance. Therefore, hybrid solutions have results comparable to single-interface solutions but are more compact.

The information to retain from these experiments on upper limb feedback are, first of all, an increased modulation of the grasping force with visual or electrotactile feedback, and a validation of the electrotactile feedback when comparing its performances to visual feedback. Secondly,

hybrid feedback comprising electrotactile and vibrotactile modalities showed good performances, comparable to results obtained with single modalities, while being more compact.

1.2.2 Invasive

Sensory feedback can also be provided in a more invasive way through implanted electrodes. In this case, an electrical signal is send directly to peripheral nerves. Even though all the articles summarized in this section are about upper-limb prostheses, it is important to provide a brief state-of-the-art of the existing invasive feedback systems.

In 2014, **Ortiz-Catalan et al.**[27] proposed an upper-limb osseointegrated prosthesis. In their article, they describe in a few words the tests performed on the feedback system. The main goal was to choose stimulation frequencies that do not lead to adaptation during long-term use. The stimulation of a small field perceived as the tip of a pen on the hand palm was repeated every day for 11 months at a current corresponding to stimulation threshold and at different frequencies. Results showed that stimulation at 8 to 10Hz allows subjects to discriminate individual pulses, stimulation above 20Hz induces a tingling sensation, due to activation of rapid adaptive fibres, and the sensation is mixed between 10 and 19Hz.

In 2015, **Raspopovic et al.**[28] proposed an invasive feedback system of 4 electrodes placed on ulnar and median nerves for a myoelectrically controlled upper-limb prosthesis. These electrodes delivered touch and pressure information measured by sensors in the thumb, index and little finger. The performances of this feedback system were quantified in five steps. First, three tests were performed to assess the voluntary modulation of force. To do so, a subject had to perform three levels of force with pinch, ulnar and palmar grasp during a single-level task (stable reaching), a press-and-relieve task (discrete reaching) and a staircase task, demanding continuous modulation of the force. Result showed a success rate of 90% and an adjustment of the force after failures, compared to an inability to produce the right amount of force without feedback. An improvement of the performances also reflected the presence of a learning process. In a second step, the subject was asked to control its grasping force by integrating several independent pressure sensory inputs from the thumb, index and little finger. This information was integrated with 93% accuracy. Thirdly, the subject was asked to recognize an object position with an exploration task, and select the most adapted grasp (among pinch, ulnar and palmar) to lift and move the object, depending on the object and its location. This step was competed with 97% accuracy. The goal of the fourth step was to determine the ability of the feedback system to recognize physical properties of the object. The subject had to grasp objects and recognize their compliance among three levels of stiffness (hard, medium and soft). After three sessions, he was able to recognize them all. The last step has as purpose to assess the ability to recognize an object shape with the feedback system. Three objects of varying shape and size were presented to the subject who had to guess the shape by palpating. This was done with 88% accuracy. The results thus showed a good control of grasping force and a good recognition of objects characteristics.

In 2016, **Oddo et al.**[17] proposed an invasive feedback system providing surface feature discrimination. This system used four piezoresistors as sensors to calculate frictional shear stress along the direction of sliding motion. The measured information was converted in spike trains used to stimulate the median nerve. Two feedback methods have been tested : microstimulation with a needle electrode stimulating the nerve for healthy subjects and four implanted electrode in median and ulnar nerves (two in each) for amputated subjects. The test were performed with, as mechanical stimulation of the fingertips, sequences of ridges and grooves with varying spatial period between 0.5 and 3mm. To quantify the results, the gratings were presented as one surface with two halves of different spatial period, with 8 possible gradients between both halves : $\pm\Delta 0.0$, $\pm\Delta 1.0$, $\pm\Delta 2.0$, $\pm\Delta 2.5$. Subjects were demanded if the second half felt coarser, finer or of same coarseness. During stimulation, the sensation felt by healthy subjects was comparable to

a mechanical stimulation of the palmar side of the first four fingers. For amputated subjects, only one electrode was activated and the sensation was comparable to mechanical stimulation of the palmar side of the index finger. Subjects reported a representation of ridges and grooves close to reality. The differentiation of the two halves was higher with implanted electrodes than with microstimulation, with a discrimination rate of 96%. This capability to discriminate showed a correlation with the gradient of spatial period. By comparing the sensation and stimulation thresholds and the ranges of electric charges needed for fibres recruitment, the conclusion was made that the results in both feedback methods could be comparable thus microstimulation can be tested to predict results of implanted electrodes.

In their article written in 2017, **Wendelken et al.**[29] proposed a solution of two arrays of 100 micro-electrodes (one on the median nerve, one on the ulnar nerve) to generate touch sensations of the hand palm. The first test to assess the feasibility of this feedback system was the creation of a stimulation threshold map. To do so, each electrode was stimulated with a pulse-train of 200ms at 200Hz and increasing amplitude until perception. The second test consisted in characterising the stimulation felt for each electrode by its location, intensity, size and quality (description of the type of sensation). Results for the first test showed that not all electrodes induced a perception since one subject (implanted in the upper arm) reported a sensation for 131 out of the 192 electrodes while the second subject (implanted in the distal forearm) sensed only 97 of the 192 electrodes. The repetition of the test over weeks also showed an augmentation of the thresholds for the second subject while no change in the median nerve but a complete adaptation of the ulnar nerve on week 5 for the first subject. During the second test, subjects showed a good discrimination of location and quality as well as a stability of the sensation over hours, but not over weeks. The number of different proprioceptive and cutaneous percepts felt by each subject was over 100.

The main results of these tests on invasive feedback methods are, first of all, that a feedback of the pressure sensed by the thumb, index and little finger delivered through electrodes on the median and ulnar nerve allows a good control of the grasping force and a good recognition of objects characteristics. Secondly, arrays of micro-electrodes on the same nerves induce sensations that are not very stable in time (especially long-term), in location or from one person to another. The stimulation indeed induces a lot of sensations of various characteristics. Finally, the comparison of two invasive feedback methods, on the median and ulnar nerves again, gave interesting results. The comparison between a microstimulation with a needle electrode and a stimulation with 4 implanted electrodes gave comparable results when inducing an impression of ridges and grooves sequences via spike trains stimulation. Needle stimulation can thus be used to predict the results obtained with implanted electrodes.

Among all the external stimulating modalities discussed in this section, electrotactile and vibrotactile feedback seem to be the most promising ones. Indeed, even though visual and auditory stimulations give good results, they are either not portable or not practical to use. Among the three tactile modalities, very few experiments have been conducted on mechanotactile feedback since the sensations that it induces are repeatable with vibrotactile stimulation. Finally, hybrid feedback also seems very promising since it gives the same results as single-modality feedbacks while being more compact.

Chapter 2

Experimental protocol

Now that the literature has been reviewed, an highlighted choice of experimental protocol can be made. In the first section of this chapter, the choice of stimulation modality will be explained. This choice is made among the two external modalities that seemed the more promising based on the literature review. The material used for the stimulation is also described and the stimulation times for the different phases of the experiment are as well chosen. In the second section, the material used for the real-time analysis of the gait is described.

2.1 Stimulation modality

The aim of this section is to define the stimulation part of the experimental protocol, containing the choice of the stimulated area, the related stimulation parameters, the stimulating device and the stimulation times for the different phases of the experiment.

2.1.1 Stimulated area

Two hypothetical stimulation points, both situated proximal to a trans-tibial amputation, will be described in this section. Their stimulation modalities will also be described with the idea of providing an augmented proprioceptive feedback of the lower limb. The anatomy and natural role of each of them will be described, followed by the stimulation modalities needed to disturb their role in the proprioception. A comparison will then be made in order to choose the area to stimulate during the experiment.

The first stimulation point is the patellar tendon, stimulated with vibrotactile stimulation, and the second one is the common fibular nerve, stimulated with electrotactile stimulation.

Patellar tendon

Anatomy The patellar tendon is the part of the quadriceps tendon connecting the apex of the patella to its distal insertion on the tibial tuberosity. It is also called patellar ligament due to its situation between two bones, while a tendon is supposed to connect a muscle and a bone. It is thus a part of the quadriceps tendon which is the distal part of the rectus femoris, one of the four muscles of the quadriceps femoris. This muscle is an extensor of the knee joint and uses the patella, situated in the middle of the quadriceps tendon, as a lever arm to increase the torque induced on the knee by the force it exerts [31][32]. The anatomy of the patellar tendon can be seen on the Figure 2.1.

Natural role While it was said earlier that the main receptors for proprioception in tendons are the Golgi tendon organs, the article [33] shows that the majority of the receptors in the patellar tendon are free nerve endings, also called neuromuscular spindles, usually found in

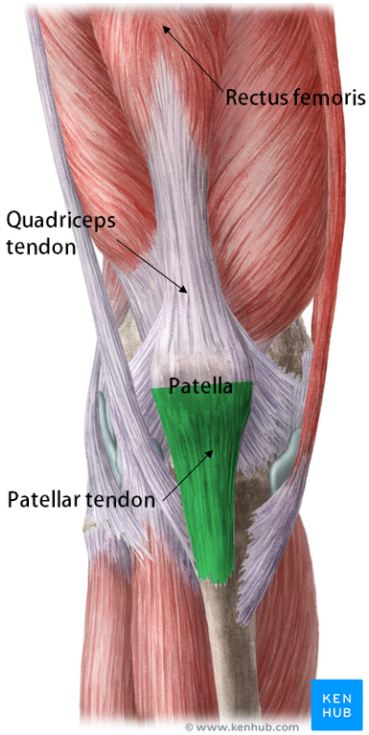

Figure 2.1: Anatomy of the patellar tendon [31].

muscles. A part of the neuromuscular spindles codes for constant tendon/muscle length while another part codes for length changes. Nerves coding for position transmit the information with a smaller firing rate than nerves giving information about movement. The frequency of these latter is also proportional to the movement velocity [34].

The patellar tendon, together with all the muscles and tendons situated around the knee, gives information about the status of the knee. Indeed, for each articulation, the whole set of muscles (with their tendons) crossing the joint contributes to the proprioceptive information perceived by the brain. The afferent information of all the muscles and tendons is thus taken into account to derive the spatial position [35]. The patellar tendon being situated around the knee, it gives information about the status of the knee and the elongation of its linked muscle, the rectus femoris.

Stimulation The stimulation modality used to provide augmented feedback to tendons is vibrotactile stimulation. In the literature, different stimulation frequencies have been tested for vibrotactile stimulation of tendons in the upper and lower limb. The article [34] describes a stimulation test of the left and right tendons of the biceps brachii at 40, 60, 80, 100 and 120Hz and reports that the frequencies inducing a movement impression with the more vividness were 40 and 60Hz. In the other hand, most articles [36, 37, 38, 39, 40] describe experiments where a stimulation frequency of 80Hz was used with a fixed amplitude parameter inducing an optimal kinetic illusion.

Common fibular nerve

Anatomy The sciatic nerve, coming from the posterior thigh, divides into the tibial nerve and the common fibular nerve, also called common peroneal nerve, when travelling through the popliteal fossa, situated in the posterior knee. The common fibular nerve then descends in an oblique way to the head of the fibula and winds around it passing to the front of the leg. This first part of the nerve path can be seen in Figure 2.2. The common fibular nerve is palpable

during its circumvention around the head of the fibula since it lies right beneath the skin.

In a second time, the common fibular nerve enters the fibularis longus muscle and divides into two branches: the superficial fibular nerve and the deep fibular nerve (see Figure 2.3). The superficial fibular nerve innervates two muscles: the fibularis longus muscle and the fibularis brevis muscle. Their main function is the eversion of the ankle and they are situated in the lateral compartment of the leg. The deep fibular nerve innervates muscles of the anterior compartment of the leg: the tibialis anterior muscle, the extensor digitorum longus muscle, the extensor hallucis longus muscle, the extensor digitorum brevis muscle, the extensor hallucis brevis and the fibularis tertius muscle. The first three muscles are, together, dorsiflexor of the ankle. The extensor digitorum longus and extensor hallucis longus are also responsible respectively for the extension of the big toe and of the 2nd to 5th toes. The last three muscles are responsible for the dorsiflexion of the foot and the fibularis tertius takes part in the eversion of the ankle. The anatomy of all the muscles cited can be seen in Figures 2.4 and 2.5.

Together, the cutaneous branches of the superficial and deep fibular nerves also provide sensory information from the dorsum of the foot (excluding fifth toe) and the lateral compartment of the leg [41][42].

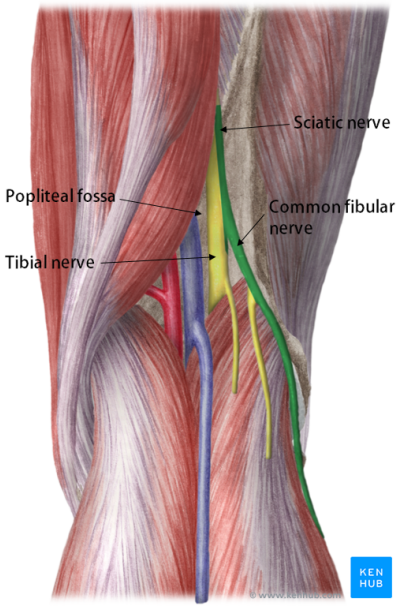

Figure 2.2: Anatomy of the common fibular nerve, back view [41].

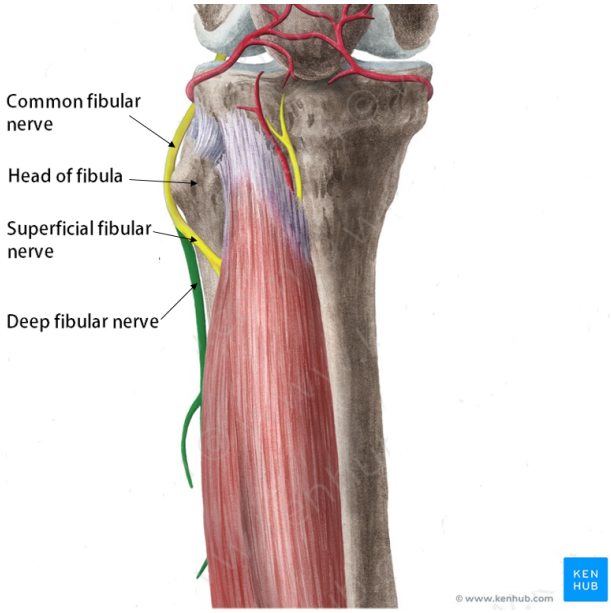

Figure 2.3: Anatomy of the common fibular nerve, front view [43].

Natural role As explained for the patellar tendon, the majority of the receptors in muscles are neuromuscular spindles that code either for position or for movement. The article [35] specifies that the activity of the common fibular nerve comes from at least 35 muscle spindles afferent from the muscles cited earlier. The activity recorded thus depends on the combined state of all the muscles, and the activity coming from each muscle depends on whether the muscle is lengthening or shortening, or in the same position for several seconds or less.

Due to the nature of the muscles innervated by the common fibular nerve, its firing rate will mainly depend on the state of eversion and dorsiflexion of the ankle.

Stimulation The stimulation modality used to provide augmented feedback to nerves is electrical stimulation. The article [47] gives the stimulation frequencies used for electrotactile stimulation of the common fibular nerve. The afferent fibres of the nerve are stimulated at about 200Hz while the efferent fibres are activated at lower frequencies like 25Hz. Since the purpose of

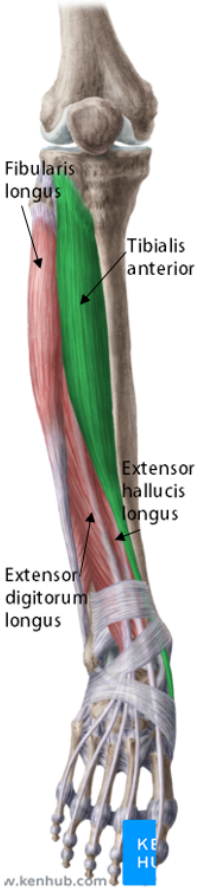

Figure 2.4: Anatomy of the fibularis longus, covering the fibularis brevis, tibialis anterior, extensor digitorum longus and extensor hallucis longus [44] .

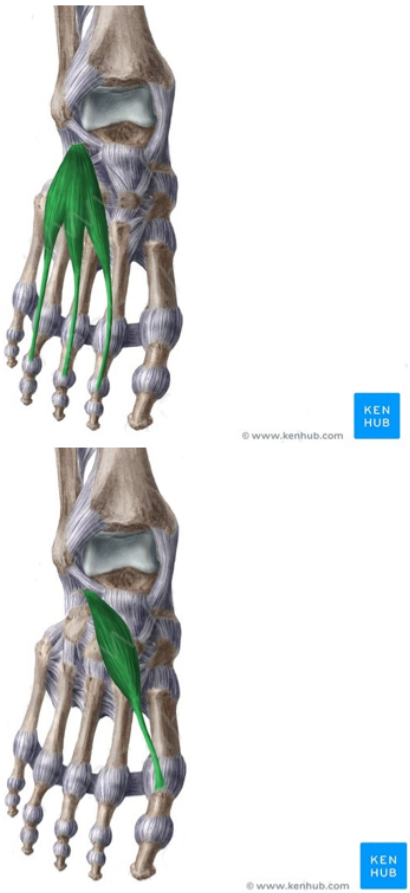

Figure 2.5: Top : Extensor digitorum brevis [45]. Bottom : Extensor hallucis brevis [46] .

the experiment is to interfere in the proprioception, the afferent fibres must be stimulated in our case.

Choice of the stimulated area

Both the patellar tendon and the common fibular nerve transmit proprioceptive information of the leg but the movement of the common fibular nerve during gait makes its stimulation less reliable contrary to the patellar tendon that only stretches and shrinks. Indeed, as stimulating electrodes are fixed on the skin, a relative movement between the nerve and the electrode would probably happen during the experiment, making the nerve not uniformly stimulated in time. The perturbation is thus more likely to happen evenly with patellar tendon stimulation and that makes the effects measured more reliable. The choice of the stimulated area is thus fixed to the patellar tendon with vibrotactile stimulation as stimulation modality.

2.1.2 Vibrotactile device

The vibrotactile device used to deliver the stimuli to the subject is the haptuator from the Tactile Labs seen in Figure 2.6 [48]. The functioning principle is the following: the vibrotactile stimuli are delivered by a recoil-type vibrotactile transducer driven by a standard audio amplifier. The transducer works following the same principle as an electromagnetic loudspeaker, and the different parts can be seen in Figure 2.7(a). A cylindrical magnet (in white) is situated at the

center of a tubular enclosure (in hashed lines) and held in place by two non-ferromagnetic pins (in hashed lines) attached to the tubular enclosure by two rubber membranes (in gray). The coil, situated around the tubular enclosure, crosses perpendicularly the magnetic field generated by the magnet. A Laplace force in the axial direction is created when the current passing through the coil interacts with the magnetic field, resulting in a displacement of the magnet in the axial direction, made possible by the suspension mechanism. The force resulting from the interaction between the current in the coil and the magnetic field is directly proportional to the input current until saturation, and the range of the frequencies of the magnet movement, thus of the stimulation frequencies, goes from a few Hz to about 500Hz [49].

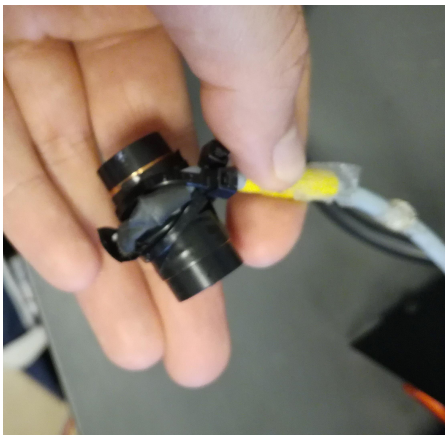

Figure 2.6: Vibrotactile unit, Haptuator, Tactile Labs, Canada.

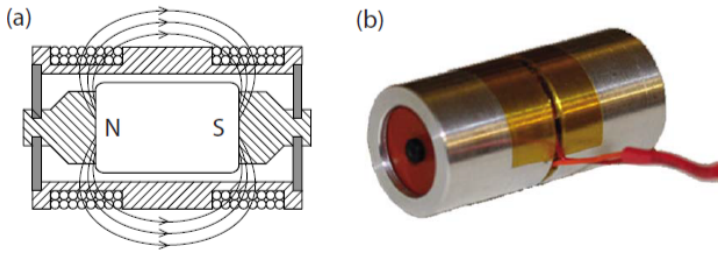

Figure 2.7: Functioning of the haptuator [49]. (a) Internal arrangement. (b) External design.

Given that the actuator is activated by a standard audio amplifier, the frequency and the amplitude must be fixed as parameters for the sound wave. Since the resonance frequency is situated around 60Hz [48], this frequency of stimulation can not be used. The stimulation frequency can thus be fixed at 80Hz since it is the most widely used frequency in the literature [36, 37, 38, 39, 40]. The amplitude can be modulated by the volume of the sound signal to be perceived by the subject but not uncomfortable.

2.1.3 Stimulation time

Even though the stimulation parameters were chosen to add proprioceptive information to the subject through the patellar tendon, the vibration is still mostly perceived by the mechanoreceptors of tactile sensitivity situated under the skin. In the literature, the zero-delay stimulation is generally provided at the same time as a specific gait event easily detectable by the subject. The purpose here is thus to provide this zero-delay stimulation at the same time as an easily identifiable gait event to make it easier for the subject to associate the stimulation to a specific gait phase. The gait event providing the bigger step in tactile feedback is the initial contact of

the foot with the ground. This time is thus chosen as the zero-delay stimulation time and the perturbation is applied as a delay relatively to the contact time. The stimulation is applied for 100ms in order to be sure that the subjects perceive it [50].

The goal of the first experiment is to prove its feasibility and give a first clue on the results that could come out by expanding it. This experiment is divided in three phases. For the first phase, called zero-delay, the subject walks on a treadmill at 3 km/h for 5 minutes and the vibrotactile stimulation is applied to his patellar tendon simultaneously with the heel-strike. The second phase, called positive-delay, consists in the same experiment but this time, the stimulation is applied 50ms after heel-strike. During the third phase, called negative-delay, the stimulation is applied 50ms before heel-strike.

2.2 Gait phase detection

In order for the stimuli to be delivered at the same gait phase for every step, the gait signal must be measured and analysed in real time. To do so, I used the Inertial Measurement Units x-IMU (x-io Technologies Limited, United Kingdom) seen in Figure 2.8. Each unit is composed of an accelerometer, a gyroscope and a magnetometer, all triple-axis, and provides therefore 9 signals. As I use these IMU to obtain gait-specific signals, the data from the accelerometer and the gyroscope are the more relevant for this application.

To acquire data, the IMUs can be connected in Bluetooth to a computer, allowing an acquisition frequency up to 128Hz. The interface is written in C# and is available in open source [51]. To treat the data in real time, detect the contact of the foot with the ground and activate the stimulation, I modified this open source code by treating the signal as explained in the next chapters.

Figure 2.8: x-IMU, x-io Technologies Limited, United Kingdom [52].

As the stimulation was provided to the subject's right leg, the IMU was placed on the right shank of the subject. The x-axis was parallel to the antero-posterior axis of the subject, the y-axis was vertical, and the z-axis was parallel to the medio-lateral axis of the subject, as illustrated in Figure 2.9. A second IMU was placed on the left shank of the subject for data acquisition. This second IMU was placed on the external side of the left shank with the same orientation as the first IMU.

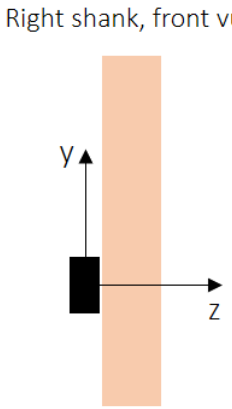

Figure 2.9: Placement of the IMU on the subject.

Chapter 3

Proof of concept

The signal received from the IMU must be treated and analysed in order to trigger the vibration at heel-strike exactly or after the defined delay. The goal of this chapter is to prove that it is feasible. To do so, it is divided in two parts: the first part describes the steps followed to robustly detect the contact time in the chosen IMU signal and the second part explains how the delays are managed in the activation of the vibration.

3.1 Contact detection

As said earlier, 9 signals are provided by the IMU to analyse the gait in real time. In order to detect the contact as precisely as possible, one of these signals must be chosen and treated. The purpose of this section is to prove that a good choice of signal combined with an appropriate treatment leads to a robust detection of the heel-ground contact.

3.1.1 Choice of the signal

As said in Section 2.2, the IMUs provide 9 signals: the linear acceleration along the 3 axis, the angular velocity around the 3 axis and the magnetic field along the 3 axis. Based on the literature [53, 54, 55, 56, 57, 58], the signal provided by the gyroscope around the z-axis, corresponding to the angular velocity of the shank around the medio-lateral axis, is chosen for real-time contact detection. Indeed, this signal shows a clear pattern, with heel-strike corresponding to a peak as seen in Figure 3.1.

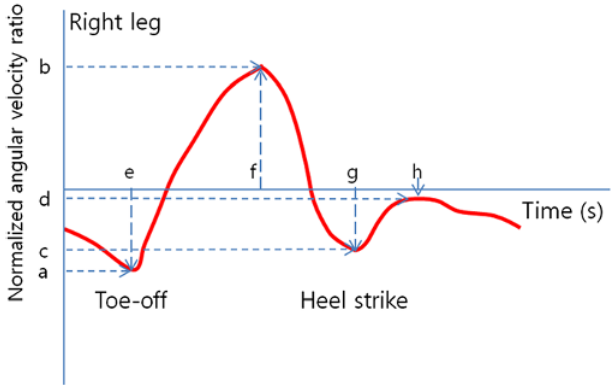

Figure 3.1: Gait phases in the angular velocity signal around the medio-lateral axis of an IMU placed on the shank [56].

The raw shank angular velocity signal obtained with the IMU oriented as define in Section 2.2

can be seen in Figure 3.2. The other 5 relevant signals (from the accelerometer and gyroscope) can be seen in Appendix A.

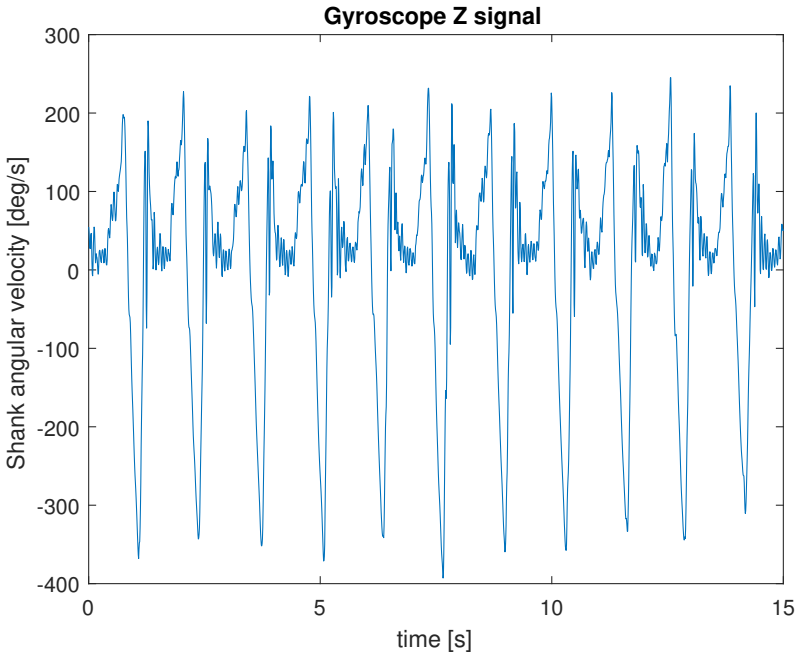

Figure 3.2: Gyroscopic signal around the z-axis.

3.1.2 Signal filtration

To reduce the noise in the signal used for contact time detection, the raw signal must be filtered in real time. To do so, a third degree Butterworth low-pass filter is applied. The cut-off frequency is determined by trial and error to decrease the risk of local maxima and is finally fixed to 5Hz.

One can see in Figure 3.3 that the data are delayed by the filter. This temporal delay will be quantified in Section 3.2.1 in order to be taken into account in the activation of the vibration.

3.1.3 Signal learning

Given that the shank angular velocity signal shows several maxima, one of the conditions for contact detection has to be based on the fundamental frequency of the signal, closely related to the step duration. Since this frequency slightly changes over time, it must be learned and adapted in real time. To do so, adaptative oscillators (AOs) are used.

Since the gyroscopic signal provided by the IMU is periodic and can be approximated by 3 harmonics, it can be easily learned by AOs as described by **Yan et al.**[59]. The fundamental features of the signal learned by the AOs in real time are the fundamental frequency ω, the phase and amplitude of each harmonic i, φ_i and α_i, and the offset component α_0. They are given by Equations 3.1, 3.2, 3.3 and 3.4 respectively.

$$\dot{\omega}(t) = \nu_\omega \frac{F(t)}{\sum \alpha_i} cos(\varphi_1(t)) \tag{3.1}$$

$$\dot{\varphi}_i(t) = \omega(t) \cdot i + \nu_\varphi \frac{F(t)}{\sum \alpha_i} cos(\varphi_i(t)) \tag{3.2}$$

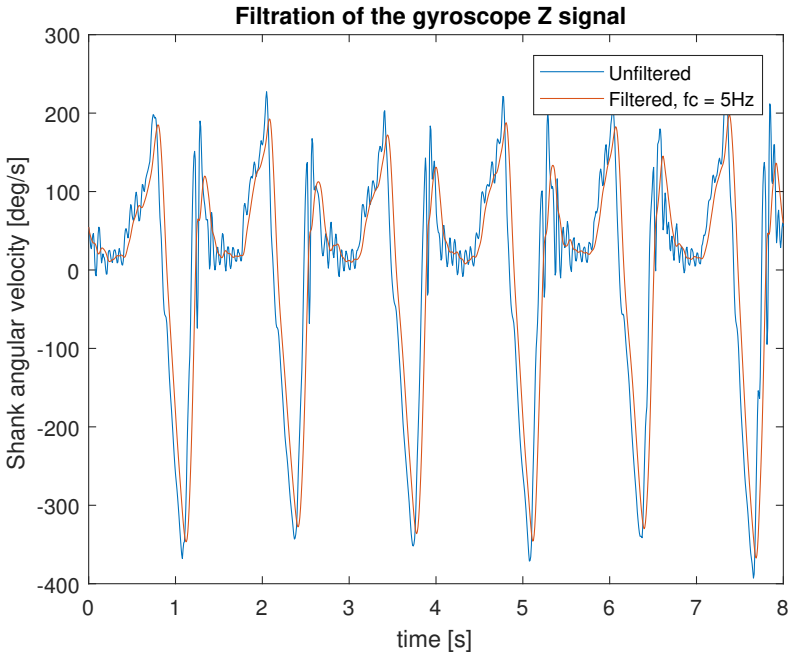

Figure 3.3: Comparison of the gyroscopic signal around the z-axis before and after filtration with a 5Hz cut-off frequency.

$$\dot{\alpha}_i(t) = \eta F(t) sin(\varphi_i(t)) \tag{3.3}$$

$$\dot{\alpha}_0(t) = \eta F(t) \tag{3.4}$$

where $F(t)$ is the difference between the input signal $\dot{\theta}$ and its estimate $\hat{\dot{\theta}}$ given by Equation 3.5.

$$\hat{\dot{\theta}}(t) = \alpha_0(t) + \sum(\alpha_i(t) sin(\varphi_i(t))) \tag{3.5}$$

By fixing the gains ν_ω, ν_φ and η to

$$\nu_\omega = \frac{10}{(2d_{step})^2}, \quad \nu_\varphi = \sqrt{24.2\nu_\omega} \quad \text{and} \quad \eta = \frac{2}{d_{step}}$$

where d_{step} is the initial step duration set to $1.2s$, and by bounding the fundamental frequency between 0.2π and 2π, the filtered signal is correctly learned, as seen in Figure 3.4.

Knowing the fundamental features of the shank angular velocity signal gives us the necessary tools for heel-strike detection, as explained in Section 3.1.4, and provides the basic signals used in delay management as explained in Section 3.2.2.

3.1.4 Contact detection

According to the literature [53, 54, 55, 56, 57, 58], the contact time of the shank angular velocity signal corresponds to the maximal peak following the minimal peak of mid-stance. This peak must be robustly found in order to deliver the stimulation at heel-strike.

A contact is detected if the three following conditions are met:

- A condition on the amplitude of the angular velocity to avoid local maxima detection:

$$\dot{\theta} > 50$$

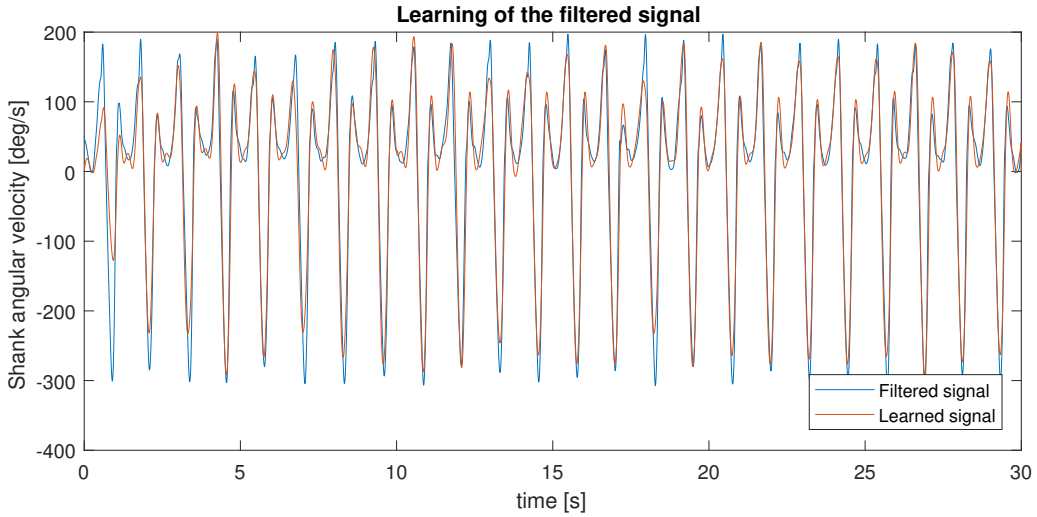

Figure 3.4: Learning of the filtered signal.

- The two conditions of a maximum:

$$\dot{\theta}_{i-1} < \dot{\theta}_i \quad \text{and} \quad \dot{\theta}_{i+1} < \dot{\theta}_i$$

- A temporal condition since the last contact time:

$$\Delta t_{contact} > \rho * \frac{2\pi}{\omega}$$

The minimal angular frequency of 50 deg/s has been fixed based on gait data analysis from several subjects. The time difference since the last contact is based on the learned fundamental frequency ω. The parameter ρ determines after what percentage of the learned step size a new contact can be found. A too weak condition will lead to the detection of the second maximum (corresponding to toe-off [53, 55, 58]) as a contact time, while a too strong condition induces a risk of non-detection. Experiments have been conducted with $\rho = 0.5$, $\rho = 0.6$, $\rho = 0.7$ and $\rho = 0.8$ on data sets acquired at 3km/h to see which condition implies the better detection rate.

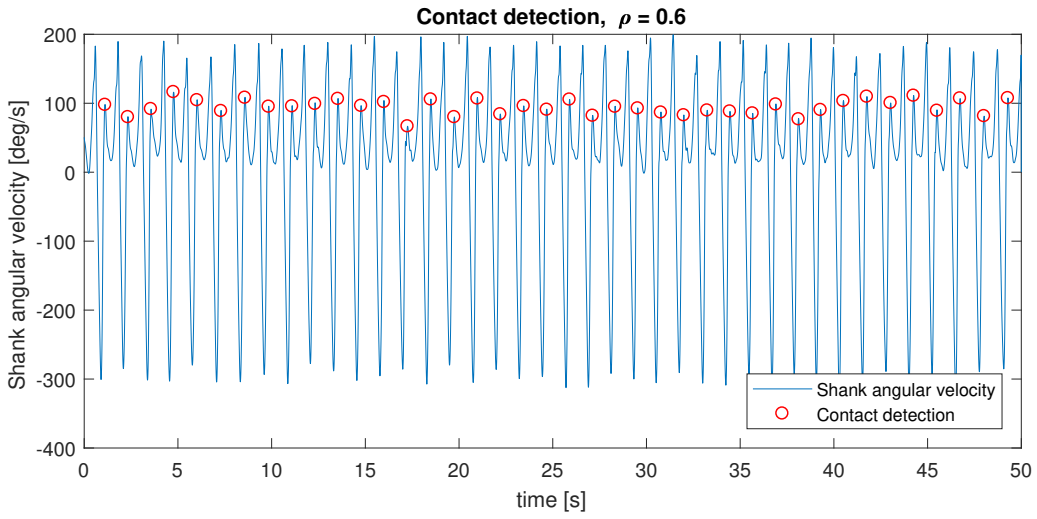

Figure 3.5: Contact detection with $\rho = 0.6$.

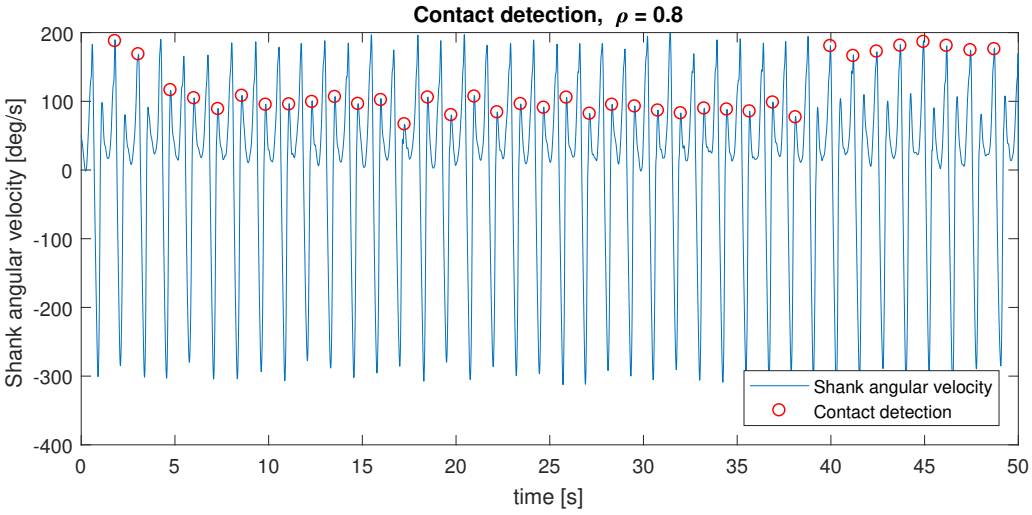

Figure 3.6: Contact detection with $\rho = 0.8$.

As seen in Figure 3.5 and 3.6, using $\rho = 0.6$ gives a 100% detection rate while $\rho = 0.8$ is a too strong condition that implies non-detection of actual contacts and detection of wrong maxima as contacts. Results with $\rho = 0.5$ and $\rho = 0.7$ are shown in Figures B.1 and B.2. One can see that $\rho = 0.5$ is a too weak condition, involving a wrong detection after 60s, while $\rho = 0.7$ gives the same results as $\rho = 0.6$. The parameter ρ is thus fixed to 0.6.

3.2 Delay management

Several delays appear between the acquisition of the signal from the IMU and the perturbation induced to the subject by the vibrotactile unit. In order for the perturbation to happen at the right gait phase, these delays must be quantified and taken into account in the activation of the stimulation. This section quantifies the delays and describes the way they are managed in the vibration activation. Table 3.1 summarizes the notations used for the different delays.

Notation	Delay
$\Delta t_{contact}$	Delay between two contact detections
Δt_{vib}	Delay between two vibration activations
Δt_{soft}	Software delay
Δt_{hard}	Hardware delay
Δt_{tot}	$\Delta t_{soft} + \Delta t_{hard}$
Δt_{exp}	Experimental delay (0, $\pm$ 50ms)
Δt_{activ}	Activation delay between contact time and vibration

Table 3.1: Summary of the notations used for the different delays.

3.2.1 Delay quantification

The delays appearing during the experiment are either due to the software (mainly the signal filtration) or to the hardware (mainly the delay between the activation of the vibrotactile unit and its vibration). They must be quantified in order to be taken into account in the activation of the vibration. Indeed, the activation of the vibration will be advanced depending of the total delay in order for the vibration to happen at heel-strike.

Software delay

As seen in Figure 3.3, the application of the low-pass filter to the signal induces a temporal delay. Since the shank angular velocity signal is delayed, the contact is detected a few milliseconds after the actual contact. The filter delay represents therefore the delay between the contact and its detection. This delay is quantified by detecting the minima of both the unfiltered and the filtered signal and by computing the mean time difference between these minima.

The minima are found based on three conditions, similarly to the maxima detection described in Section 3.1.4:

- A condition on the amplitude of the angular velocity to avoid local minima detection:

$$\dot{\theta} < -250$$

- The two conditions of a minimum:

$$\dot{\theta}_{i-1} > \dot{\theta}_i \quad \text{and} \quad \dot{\theta}_{i+1} > \dot{\theta}_i$$

- A temporal condition in the form of a number of data since the last minimum:

$$\Delta i > 100$$

The minima detection can be verified graphically as in Figure 3.7.

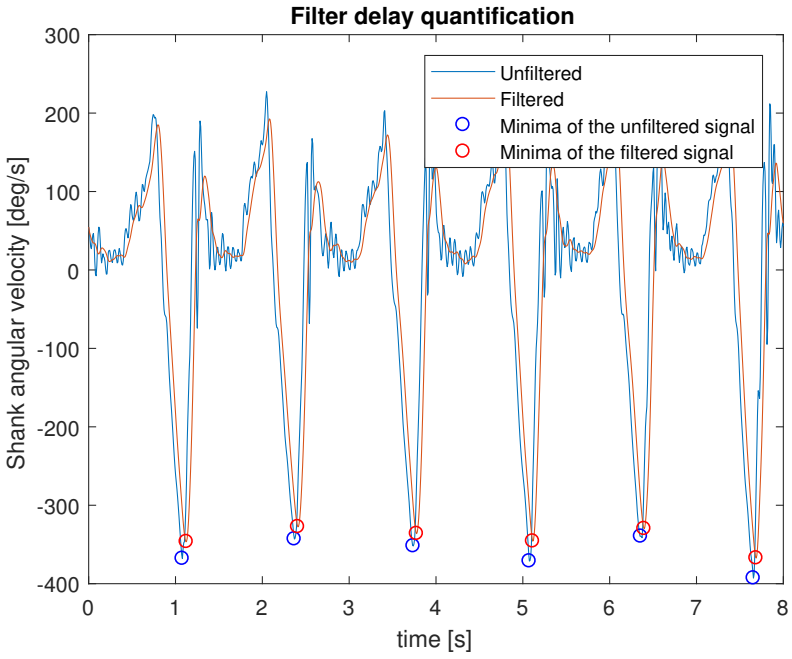

Figure 3.7: Determination of the temporal delay induced by the low-pass filter.

By computing the mean temporal delay of a large data set, we find:

$$\Delta t_{soft} = 0.041s$$

Hardware delay

When the vibration is activated in the code, a delay occurs before the actual vibration of the vibotactile unit. This delay is due to the travel of electrical signals through the hardware. To quantify this hardware delay, a second IMU was placed in contact with the vibrotactile unit and fixed to a stable surface (see Figure 3.8). The sound signal used for the vibration was chosen to be easily detectable by the IMU and the code was modified to register the times of vibration activation. The subject was then asked to walk on a treadmill. By comparing the activation times of the vibrations by the first IMU and the detection times by the second IMU (as seen in Figure 3.9), the hardware delay can be quantified. The signal of the second IMU chosen for this analysis, after comparison of the relevant 6 signals, was the acceleration in the z-direction.

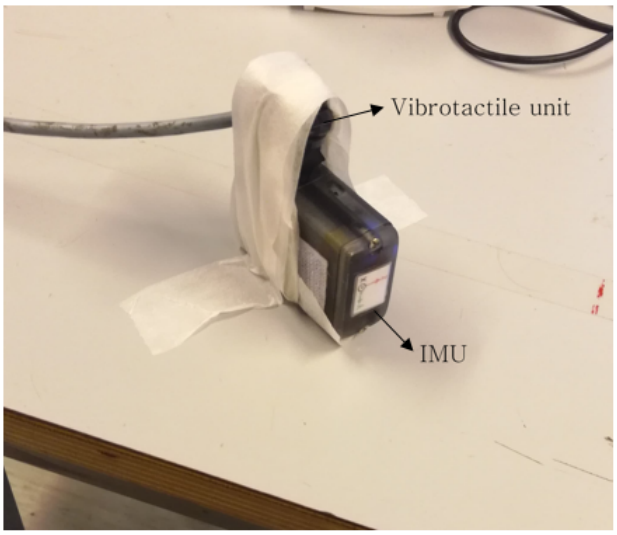

Figure 3.8: Second IMU and vibrotactile unit placement for hardware delay quantification.

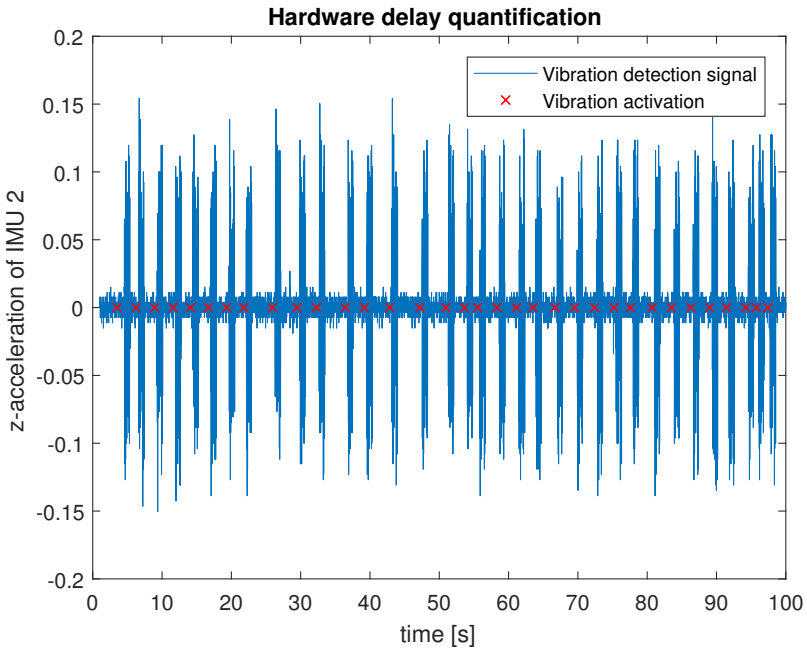

Figure 3.9: Determination of the hardware delay by comparison of the activation and detection times.

The mean time between the vibration activation and detection, thus the mean temporal delay, is $\Delta t_{hard} = 0.1923s$. The standard deviation is calculated to verify that the delay is not too different from one vibration to another and it is worth $\sigma = 0.0388s$. The hardware delay is thus quite variable. Since we take the mean delay into account in the conditions of vibration activation, one must keep in mind that this activation time will not always be optimal. Indeed, the unit could vibrate up to 40ms after the desired vibration time.

The mean total delay between the actual contact time and the vibration when it is activated by heel-strike detection is thus

$$\Delta t_{tot} = \Delta t_{soft} + \Delta t_{hard} \simeq 0.233s$$

3.2.2 Delay management

As said earlier, both the filter delaying the signal and the hardware delaying the vibration play a part in the delay occurring between the contact time and the stimulation time. In order for the stimulation to happen simultaneously with the contact, a negative delay must be added to the activation of the vibration to counteract this delay. Moreover, and as explained in Section 2.1.3, the perturbation is given as a late or early stimulation compared to the zero-delay condition. This experimental delay Δt_{exp} (positive for a late stimulation and negative for an early one) must be added to the vibration activation time. The delay between the contact time and the activation time is given by

$$\begin{aligned} \Delta t_{activ} &= -\Delta t_{tot} + \Delta t_{exp} \\ &= -0.233s + \Delta t_{exp} \end{aligned}$$

If this delay is negative, we make the hypothesis that the step duration is relatively constant and that the next step duration will therefore be close to the mean step duration. We define the activation time as

$$\begin{aligned} \Delta t_{activ} &= d_{step} - \Delta t_{tot} + \Delta t_{exp} \\ &= d_{step} - 0.233s + \Delta t_{exp} \end{aligned}$$

The step duration d_{step} is computed at each contact time as the mean of all the previous step durations (see Equation 3.6). The initial step duration is fixed at $1.2s$.

$$d_{step,new} = \frac{d_{step,last} * (n-1) + \Delta t_{contact}}{n} \tag{3.6}$$

with n the number of steps.

Based on the features learned by the AOs (see Section 3.1.3, Equations 3.1 and 3.2), a phase reset signal ϕ can be computed in real time and used as a condition to activate the vibration. This signal, given by Equation 3.7, increases from 0 to 2π between two contact times. Its increase is due to the phase error φ_e depending on the fundamental frequency ω and on the difference between the current time t and the last contact time t_k, as seen in Equation 3.8. It also depends on the error signal ε computed at each contact time and given by Equation 3.9 [59].

$$\phi(t) = mod(\varphi_1(t) - \varphi_e(t), 2\pi) \tag{3.7}$$

$$\dot{\varphi}_e(t) = \varepsilon(t_k)\omega e^{-\omega(t-t_k)} \tag{3.8}$$

$$\varepsilon(t_k) = 0.3(mod(\varphi_1(t_k), 2\pi) - \varphi_e(t_k)) \tag{3.9}$$

The relation between the phase reset signal ϕ and the time since the last contact $(t - t_k)$ is given by Equation 3.10.

$$\omega(t - t_k) = \phi \tag{3.10}$$

As seen in Figure 3.10, $\frac{\phi}{\omega}$ increases from 0 to d_{step} during each step. This function can therefore be used to add a delay between the contact time and the vibration activation.

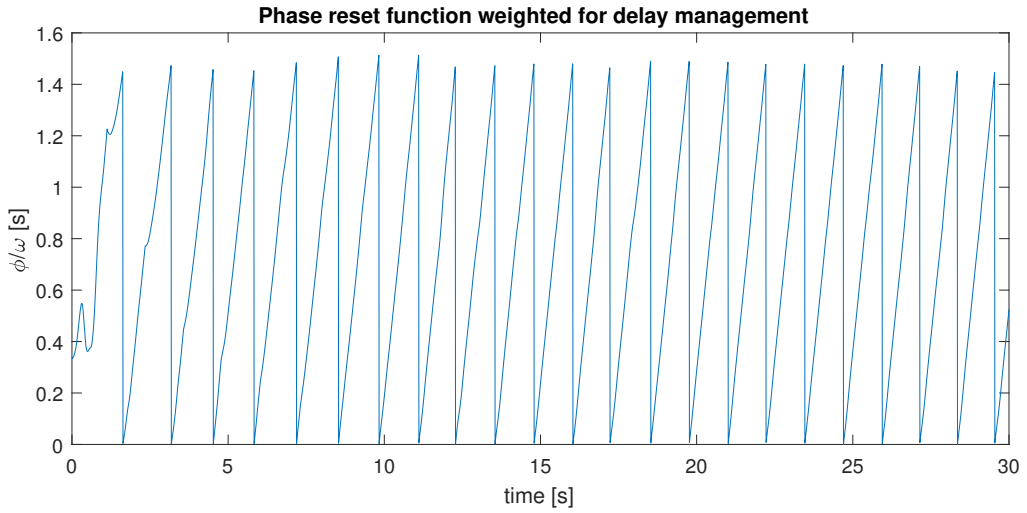

Figure 3.10: $\frac{\phi}{\omega}$ signal used for delay management. The signal increases from 0 to d_{step} between two contact times.

By using this signal, we can define the conditions of vibration activation as follows:

- The time since the last contact time is greater or equal to the delay:

$$\frac{\phi}{\omega} \geq \Delta t_{activ}$$

- The time since the last contact time is not greater than the delay + 2 sampling periods, to avoid a double activation:

$$\frac{\phi}{\omega} < \Delta t_{activ} + 2T_s$$

  with T_s the sampling period.

- A temporal condition since the last vibration activation:

$$\Delta t_{vib} > \rho * \frac{2\pi}{\omega}$$

  The parameter ρ used here is the same as for contact detection.

The first two conditions ensure the delay between the contact detection and the vibration activation while preventing a double vibration activation between two contacts. Indeed, for short delays, the $\frac{\phi}{\omega}$ signal is still on its increasing phase when the third condition becomes true. $\frac{\phi}{\omega}$ is thus still greater than the activation delay Δt_{activ} and the vibration would be re-activated without the second condition.

The application of these conditions for a 0.05 seconds activation delay can be verified in Figure 3.11. The first vibrations are not activated after the correct delay due to the learning time of the signal parameters.

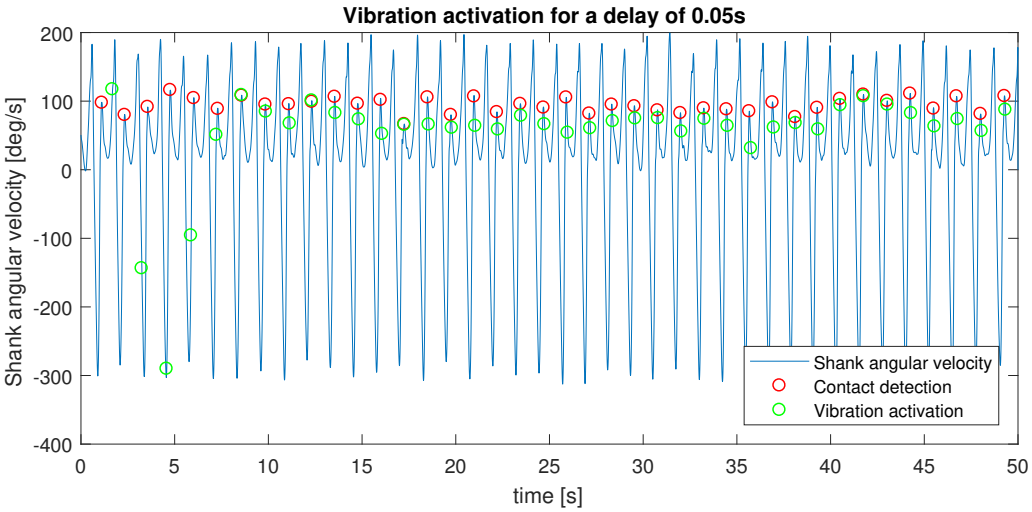

Figure 3.11: Vibration activation with a delay of 0.05s after contact detection.

Since the IMU interface is written in C#, all these signal treatments and conditions have been added to the open source code to be applied to each data of the gyroscopic signal received from the IMU. The activation of the sound signal for the vibrotactile unit has also been added under the condition of vibration activation hereabove and a function to register the contact times has been written.

Chapter 4

Results

For the first experiment, a healthy 22 years old woman walked on a treadmill at 3 km/h with the vibrotactile unit fixed with tape to her knee facing the patellar tendon, a first IMU fixed with tape to her right shank and a second IMU fixed with tape to her left shank. The IMUs were connected to a computer via Bluetooth and the data from the first IMU were analysed in real time to activate the vibration at heel-strike or after a fixed delay. This chapter gives the results of the first analysis of the data obtained.

4.1 First analysis

The first analysis consists in verifying the contact detection. Unfortunately, even though the algorithm worked on test data sets, too many mis-detections happened during this experiment, making the results inoperable. Indeed, as seen in Figure 4.1, local maxima were detected from the start, leading to detection of wrong maxima happening more than $\rho * \frac{2\pi}{\omega}$ later.

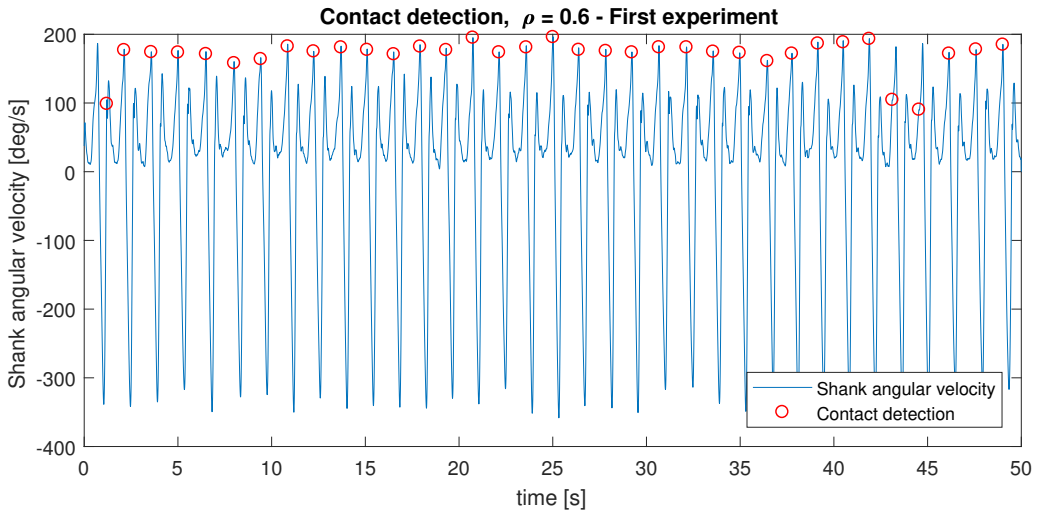

Figure 4.1: Contact detection during the first experiment.

Several solutions are proposed to improve this detection rate. They are described hereafter with the results obtained by applying them on many data sets. These solutions will then be criticized in Chapter 5 in order to point out their weaknesses and increase the robustness of the final solution.

4.2 Solutions

Two solutions are proposed here to increase the robustness of contact detection. The first solution consists in applying a stronger low-pass filter to the signal and the second solution consists in a detection of minima instead of maxima of the shank angular velocity. A third solution is then proposed to increase the robustness of the first solution. Lots of data have been acquired during the first experiment in order to test the algorithms and detect their weaknesses.

4.2.1 Smaller cut-off frequency

The first solution would be to decrease the cut-off frequency of the low-pass filter to avoid the detection of local maxima seen in Figure 4.1. The new cut-off frequency applied in real time to the data is determined by trial and error and fixed to 3Hz. A trial and error approach is also used to fix the parameter ρ and the solution is tested at different walking speed. The results for the different conditions are given hereafter and the new filter delay is then computed.

Results

This new contact detection method is first applied on sets of data at 3km/h. By fixing $\rho = 0.6$, the method gives a 100% detection rate in most cases as seen in Figure 4.2. It is also applied on data obtained at 4 and 5km/h and gives the same results, needing a modification of the initial step duration at 5km/h to 1s. The contact detection at 4km/h and 5km/h can be seen in Figures C.1 and C.2 respectively. The use of $\rho = 0.7$ induces too many mis-detection as seen in Figure 4.3.

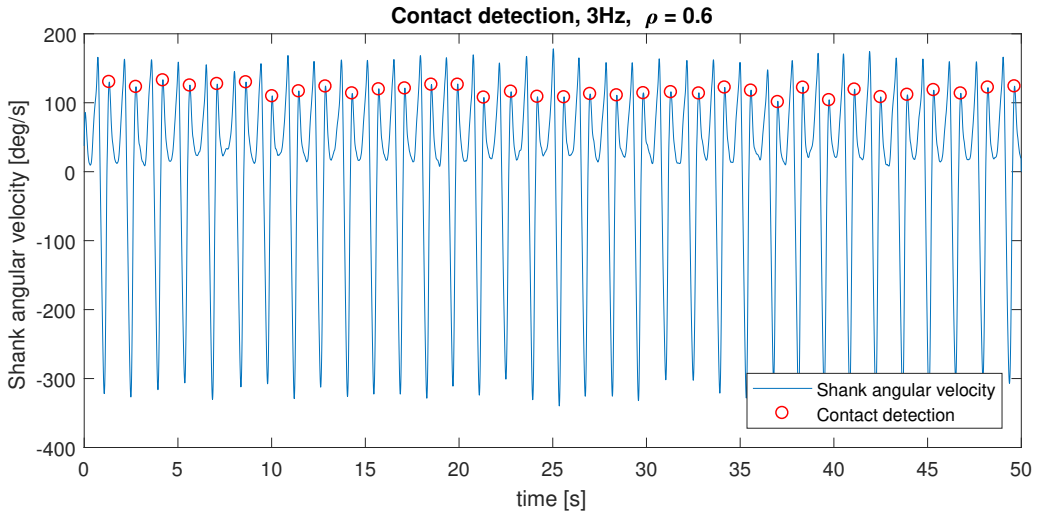

Figure 4.2: Contact detection with $f_c = 3$Hz and $\rho = 0.6$.

As seen in Figure 4.4, contact detection with $\rho = 0.6$ does not work for one data set acquired at 4km/h. The weakness of the algorithm leading to this mis-detection will be discussed in Section 5.1.1.

Delay quantification

Since the cut-off frequency of the low-pass filter has been changed from 5Hz to 3Hz, the delay between the unfiltered and the filtered signal must be re-computed. By following the same steps as in Section 3.2.1, we find :

$$\Delta t_{soft} = 0.0625s$$

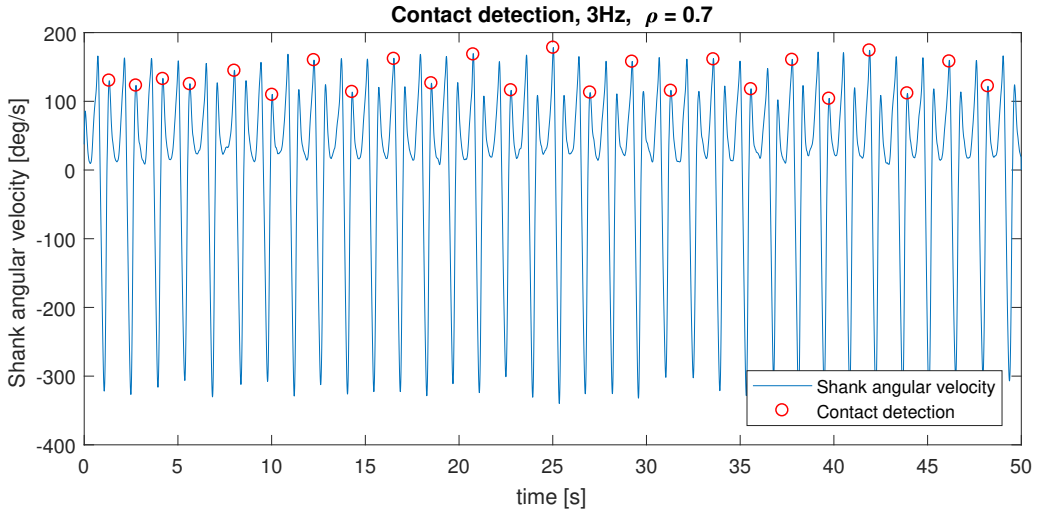

Figure 4.3: Contact detection with $f_c = 3$Hz and $\rho = 0.7$.

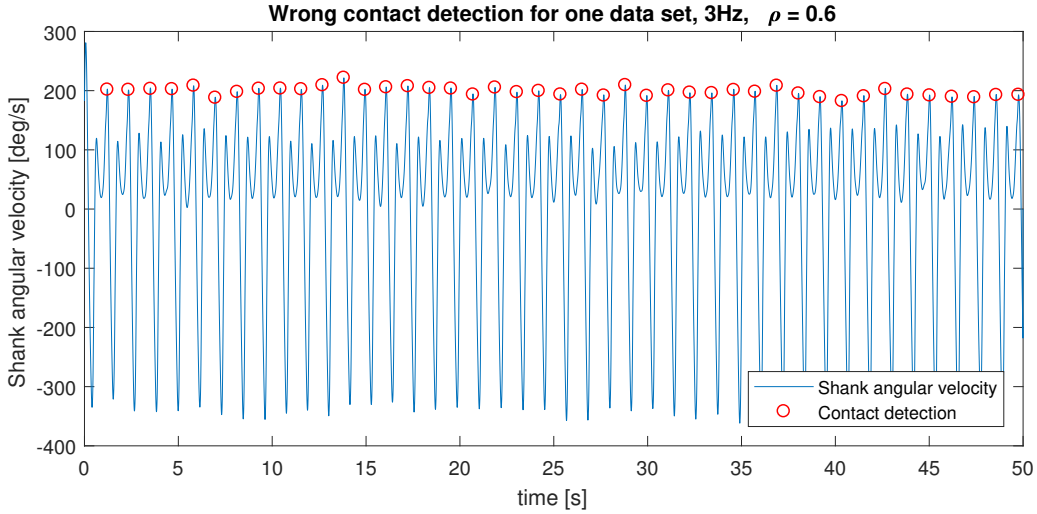

Figure 4.4: Wrong contact detection with $f_c = 3$Hz and $\rho = 0.6$.

The delay is thus bigger than the delay induced by a cut-off frequency of 5Hz as it can be seen in Figure 4.5. Combined with the hardware delay computed earlier, we find

$$\Delta t_{tot} \simeq 0.255s$$

4.2.2 Minima detection

Another solution would be to detect the minima of the signal, corresponding to the mid-swing phase of the gait [53, 55, 58], instead of the maxima corresponding to heel-strike. Indeed, given that there is only one minimum per step versus two maxima, the risk of mid-swing mis-detection is lower. The delay between mid-swing and heel-strike must be computed to be taken into account in the activation of the vibration. Indeed, the phase reset function illustrated in Section 3.2.2 will be shifted by this delay since the variable t_k will be updated at mid-swing instead of heel-strike.

The conditions used to detect the minima are similar to the ones used to compute the delay between the raw signal and the filtered signal:

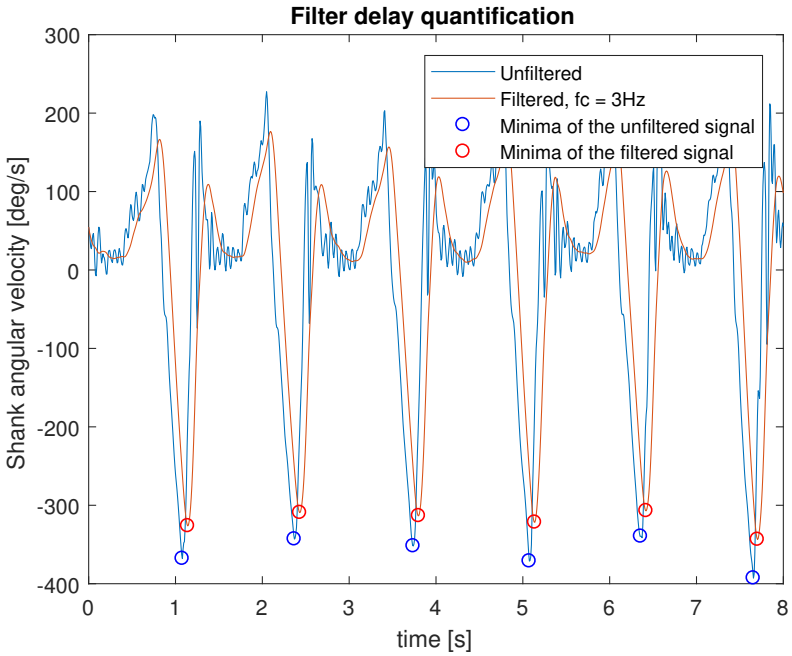

Figure 4.5: Determination of the temporal delay induced by a low-pass filter with cut-off frequency of 3Hz.

- A condition on the amplitude of the angular velocity to avoid local minima detection:

$$\dot{\theta} < -250$$

- The two conditions of a minimum:

$$\dot{\theta}_{i-1} > \dot{\theta}_i \quad \text{and} \quad \dot{\theta}_{i+1} > \dot{\theta}_i$$

- A temporal condition since the last minimum:

$$\Delta t_{min} > \rho * \frac{2\pi}{\omega}$$

Results

By applying the algorithm to several data sets, including the data obtained during the first experiment, and with $\rho = 0.6$, a 100% detection rate is obtained, as seen in Figure 4.6. $\rho = 0.7$ induces mis-detections like with the maxima detection algorithm (see Figure 4.7). By decreasing ρ in the other hand, we find a 100% detection rate for any ρ. Finally, the detection rate is still 100% after removing the condition on Δt_{min} depending on ρ, as seen in Figure 4.8. The detection conditions are thus stronger for minima detection than for maxima detection.

Delay quantification

The time between mid-swing and heel-strike must be calculated as a function of the step duration to be taken into account in the vibration activation. Indeed, the phase reset signal increases from 0 to 2π between two detected events and, as the event detected here happens x seconds before the contact, this function will be shifted by this delay and start increasing x seconds earlier. The delay computed here will thus be subtracted from the delay Δ_{tot} computed in the calculation of the activation delay.

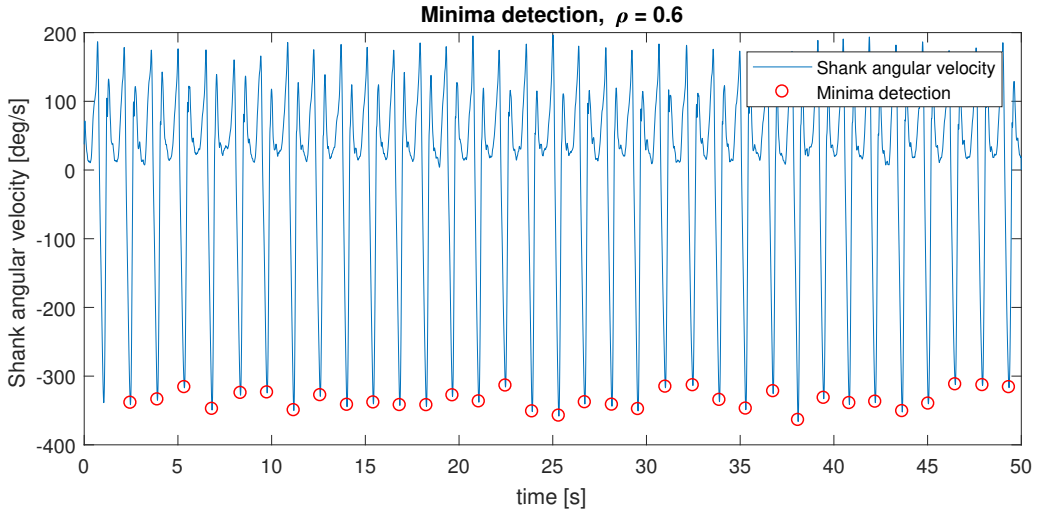

Figure 4.6: Minima detection with $\rho = 0.6$.

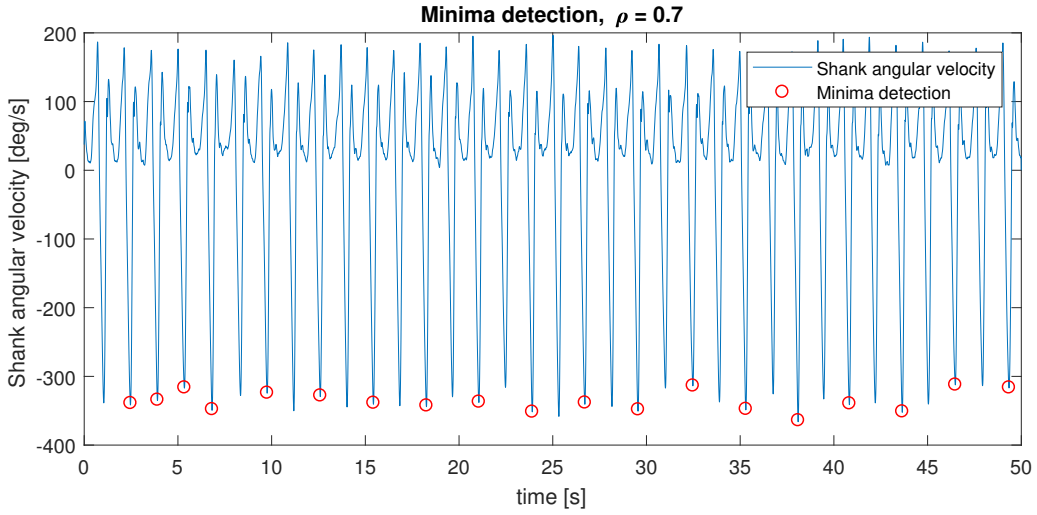

Figure 4.7: Minima detection with $\rho = 0.7$.

This delay is computed as a fraction of the step duration. To do so, minima and maxima of the shank angular velocity are detected in several data sets (as in Figure 4.9) and their mean time difference is divided by the respective mean step duration. This gives a delay of 18% of the step duration:

$$t_{contact} - t_{min} = 0.18 d_{step}$$

By taking into account the total delay (comprising hardware and software delay) computed in Section 3.2.1, the experimental delay and the minima-maxima delay, the delay between the mid-swing detection and the vibration activation is given by

$$\begin{aligned} \Delta t_{activ} &= (t_{contact} - t_{min}) - \Delta t_{tot} + \Delta t_{exp} \\ &= 0.18 d_{step} - 0.233 s + \Delta t_{exp} \end{aligned}$$

or, for a negative delay

$$\begin{aligned} \Delta t_{activ} &= d_{step} + (t_{contact} - t_{min}) - \Delta t_{tot} + \Delta t_{exp} \\ &= d_{step} + 0.18 d_{step} - 0.233 s + \Delta t_{exp} \\ &= 1.18 d_{step} - 0.233 s + \Delta t_{exp} \end{aligned}$$

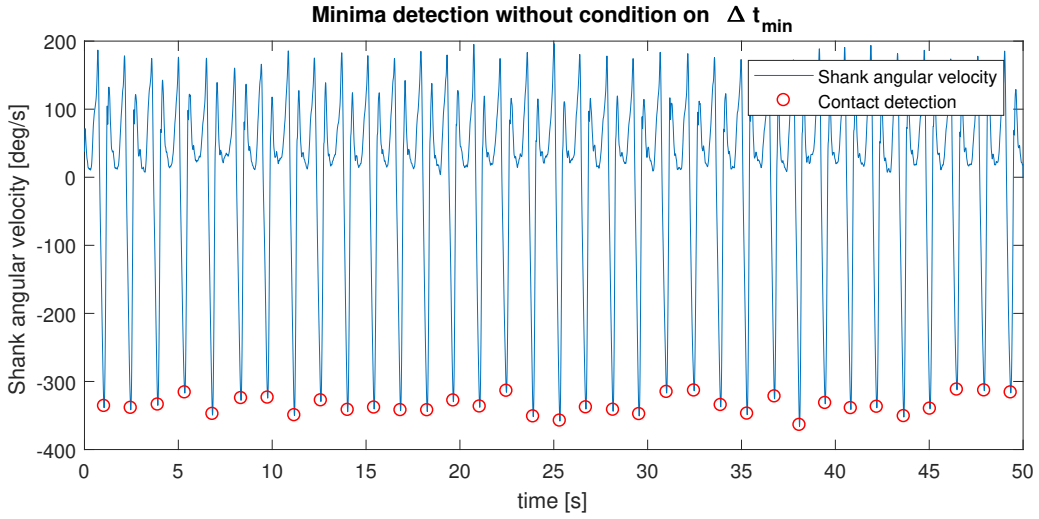

Figure 4.8: Minima detection without condition on Δt_{min}.

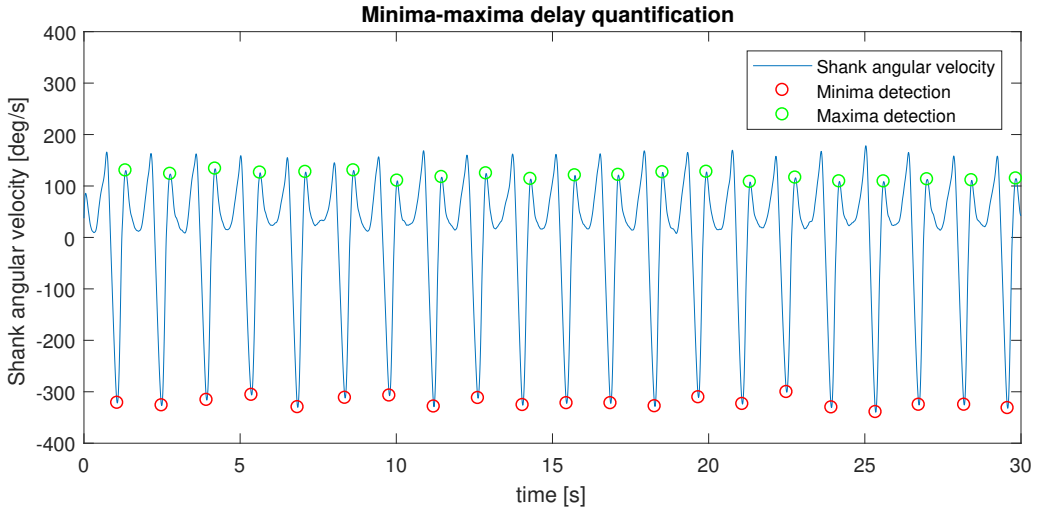

Figure 4.9: Delay quantification between minima and maxima.

4.2.3 Detection conditions

In both cases, the detection algorithm does not work for ρ higher than 0.6. To understand why, I plotted the fundamental frequency learned by the AOs and the frequency computed with the step size at each contact detection, $\frac{2\pi}{d_{step}}$. As seen in Figure 4.10, the value of the learned frequency is smaller than the value of the computed frequency. This difference is probably due to the fact that the shank angular velocity signal is too complicated to be perfectly learned by 3 oscillators, and the fundamental frequency is therefore underestimated. The time condition between two steps is thus higher than the actual time between two steps when ρ is higher than 0.6.

By modifying the gains ν_ω, ν_φ and η used in Equations 3.1, 3.2, 3.3 and 3.4 to try and learn a fundamental frequency closer to the real frequency, the variability of ω only increased, which made the condition depending on it less reliable. To have a detection condition closer to the real frequency, the condition on ω can thus be changed to depend directly on the step duration d_{step}. This change is made for maxima detection only since it has been shown that the time condition Δt_{min} can be removed for minima detection.

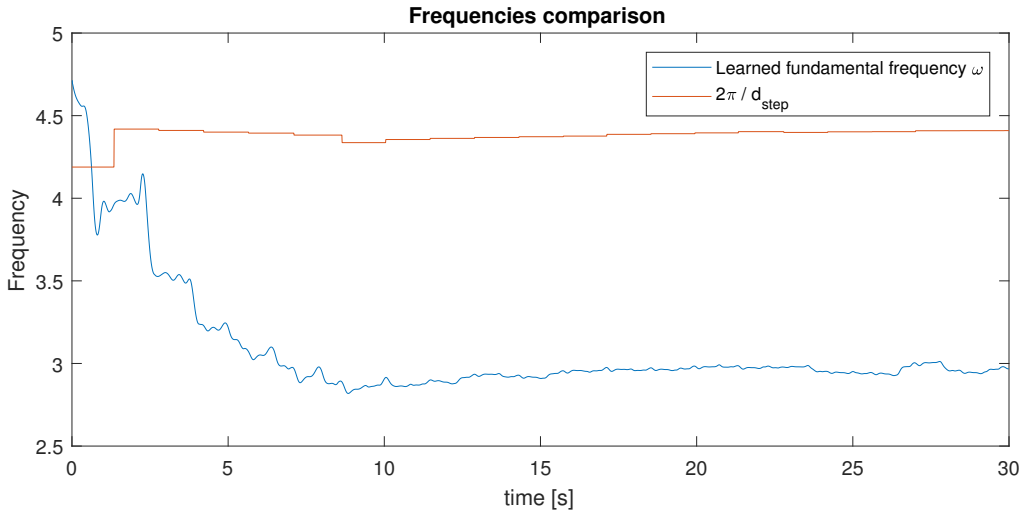

Figure 4.10: Comparison of the learned fundamental frequency ω and the computed frequency $\frac{2\pi}{d_{step}}$.

The time condition

$$\Delta t_{contact} > \rho * \frac{2\pi}{\omega}$$

is thus replaced by

$$\Delta t_{contact} > \rho * d_{step}$$

with d_{step} learned by Equation 3.6. After analysis of the data sets acquired during the experiment, the initial step duration is fixed at 1.4s for walking speeds of 3km/h.

Results

By making the parameter ρ vary for this new condition, we obtain a 100% detection rate for $\rho = 0.7$ (see Figure 4.11) while the algorithm does not work for $\rho = 0.6$ (see Figure 4.12), contrary to the results obtained with the former condition. By increasing ρ, we find mis-detections from $\rho = 0.9$ (see Figure 4.13).

The results for higher velocities are similar than with the former condition and the algorithm did not work either on the same data set.

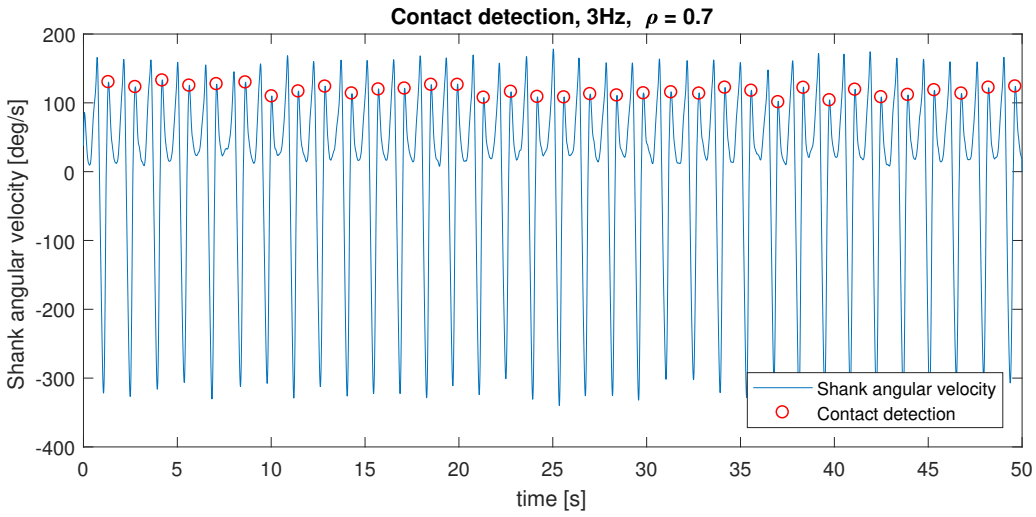

Figure 4.11: Contact detection with conditions based on d_{step}, $f_c = 3$Hz and $\rho = 0.7$.

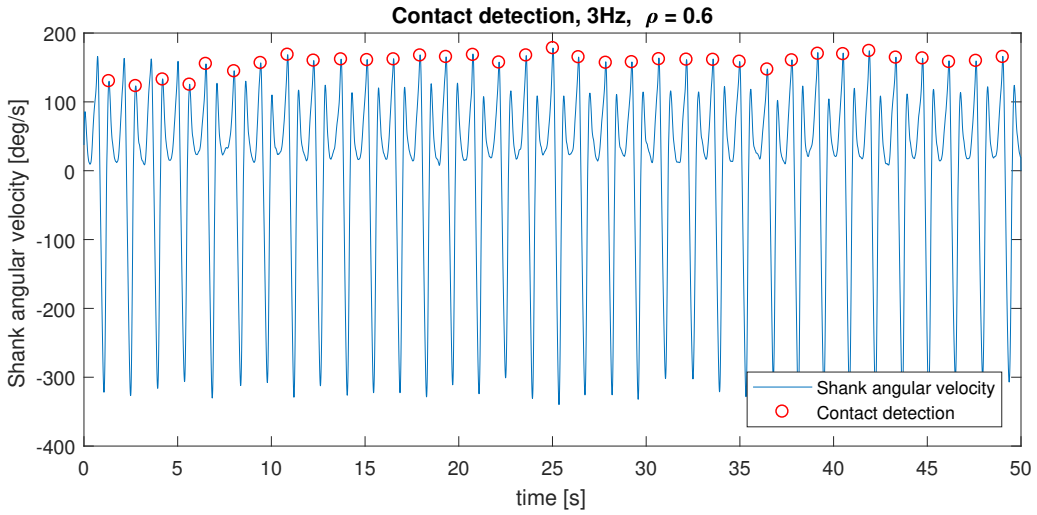

Figure 4.12: Contact detection with conditions based on d_{step}, $f_c = 3$Hz and $\rho = 0.6$.

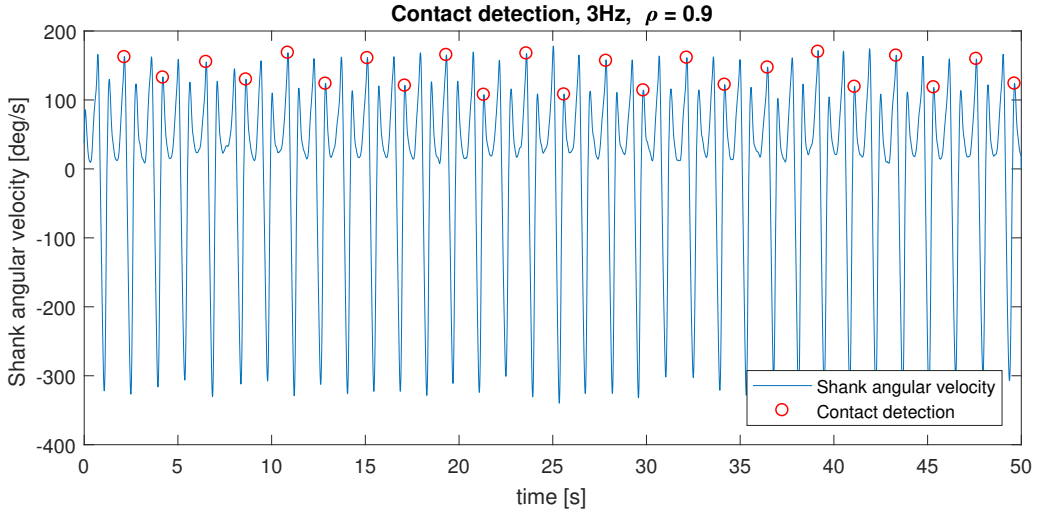

Figure 4.13: Contact detection with conditions based on d_{step}, $f_c = 3$Hz and $\rho = 0.9$.

4.2.4 Impact on delay management

As the condition for delay activation also depends on ω, it should be more precisely analysed. By comparing the weighted phase reset function $\frac{\phi}{\omega}$ with the learned step duration d_{step} (see Figure 4.14), we see that the function does not actually increase from 0 to d_{step}. The activation condition $\frac{\phi}{\omega} \geq \Delta t_{activ}$ is thus invalid, leading to advanced vibrations. The same changes than in the maxima detection conditions are thus made.

A more precise analysis of the $\frac{\phi}{2\pi} * d_{step}$ signal also reveals that the value of the signal is not always null at contact time or $2T_s$ seconds later. This leads to the modification of the second condition.

After these modifications, the conditions of vibration activation become:

- The time since the last contact time is greater than the delay:

$$\frac{\phi}{2\pi} * d_{step} \geq \Delta t_{activ}$$

- The time since the last contact time is not greater than the delay + half a step duration,

to avoid a double activation:

$$\frac{\phi}{2\pi} * d_{step} < \Delta t_{activ} + \frac{d_{step}}{2}$$

- A temporal condition since the last vibration activation:

$$\Delta t_{vib} > \rho * d_{step}$$

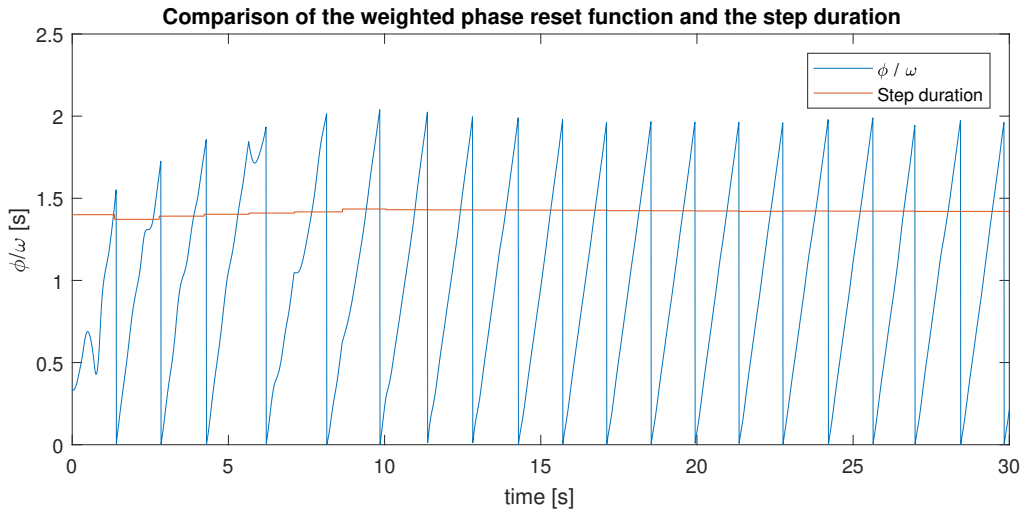

Figure 4.14: Comparison of the $\frac{\phi}{\omega}$ signal used for delay management with the mean step duration computed at each contact.

The test of the new algorithm with the contact detection conditions described in Section 4.2.3, the vibration activation conditions described hereabove, and an activation delay of 50ms gives the result seen in Figure 4.15. As for the results illustrated in Figure 3.11, the first vibrations are not activated after the correct delay due to the learning time of the signal parameters.

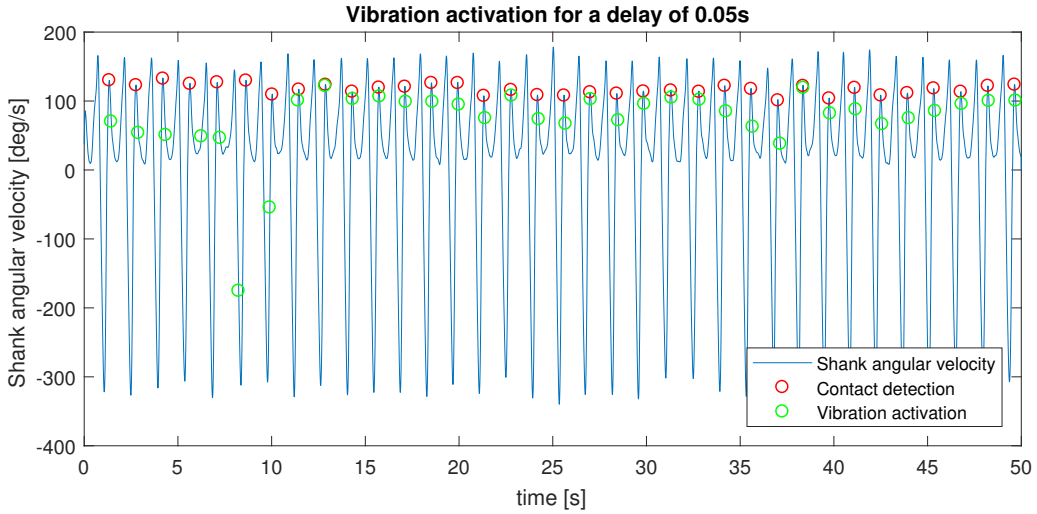

Figure 4.15: Vibration activation with a delay of 0.05s after contact detection.

Chapter 5

Discussion

After explaining the results obtained with the first experiment as well as different solutions to overcome the problems met with the first version of the code, the final solution must be chosen. Therefore, this chapter will discuss the weaknesses of the proposed solutions and explain the choice made for the second experiment. A short description of the data analysis planned follows as well as a discussion on the expected results.

5.1 Feasibility of the experiment

This section will discuss the weaknesses of each of the proposed solutions and lead to the choice of one of them for the final experiment. The weakness of the delay management method will also be discussed.

5.1.1 Weakness analysis

The weaknesses of each of the three solutions described in Section 4.2 will be described in this section. Some weaknesses have already been highlighted by the test of the algorithm on existing data sets while other are predictions of what could happen with new data. This weakness analysis will provide a clear vision of the three solutions in order to make a highlighted choice for the final solution.

Smaller cut-off frequency

The main weakness of this detection method is its dependency on the starting time of the experiment. Indeed, given that the time condition $\Delta t_{contact} > \rho * \frac{2\pi}{\omega}$ to detect the first maximum is given relatively to the starting time t_0, the first contact time will be wrongly detected if the experiment starts more than $\rho * \frac{2\pi}{\omega}$ seconds before the first maximum but less than $\rho * \frac{2\pi}{\omega}$ seconds before the first heel-strike. This situation happened with one data set and can be seen in Figure 4.4. One can see that a wrong start induces the detection of wrong maxima for the rest of the experiment.

Minima detection

The main weakness of the minima detection algorithm, and more precisely of its vibration activation, is the variation of the delay between mid-swing and heel-strike. Indeed, this delay is approximately 18% but is slightly variable from one step to another, and from one data set to another. By computing the standard deviation of the delay in one data set, we find $\sigma = 0.0122s \simeq 0.009 * d_{step}$, thus one twentieth of the delay. This delay uncertainty combined with the uncertainty on the hardware delay increases the risk of having vibrations non-concomitant with heel-strike.

Detection conditions

The main weakness of this method is the dependency of the detection condition on the detection itself. Indeed, the step duration is updated at each new detection, meaning that in case of wrong detection, the step duration will be wrongly updated and the condition for the next detection will be impacted. One wrong detection could therefore affect the detections of the rest of the experiment.

Delay management

As explained in Section 3.2.1, the hardware delay is very variable. Indeed, for a mean delay of 0.1923s, the standard deviation is $\sigma = 0.0388$s. The vibration for a zero-delay could thus happen nearly 0.04 seconds after heel-strike, closer to the experimental delay $\Delta t_{exp} = 0.05s$ than to the zero-delay condition. The boxplot in Figure 5.1 illustrates the distribution of hardware delays among 100 variables. We can see that half the delays are situated in a range of about 0.02s around the mean, which is still a reasonable deviation. 25% are smaller and do not deviate of more than 0.02s from the mean. Their deviation is thus worth nearly half the experimental delay. The last 25% deviations are comprise between 0.01s and nearly 0.04s from the mean, which is very close to the experimental delay. A large portion of the delays is thus close to this delay, making the mean delay used not very reliable. This distribution is not really reassuring compared to the standard deviation.

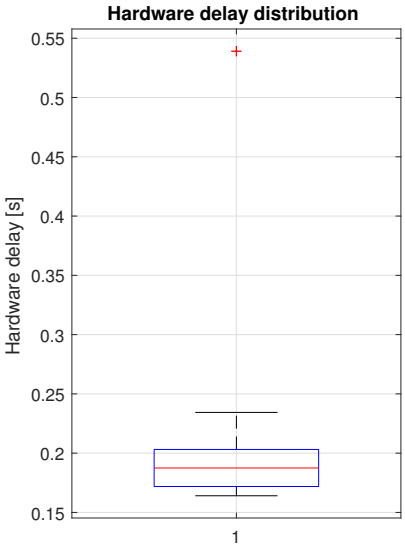

Figure 5.1: Hardware delay distribution.

5.1.2 Choice of the solution

The three solutions proposed in Section 4.2 together with their weaknesses are summarized in Table 5.1 to allow a highlighted choice for the final experiment. Even though the minima detection solution seems to be more robust than the maxima detection, the variability of the delay between minima and maxima makes it less convenient for the experiment. Maxima detection in a signal filtered at 3Hz is therefore chosen. To not rely on detection conditions based on a wrongly learned fundamental frequency, the detection and vibration conditions chosen are the ones based on step duration. To overcome the weakness of the detection conditions described hereabove, the step duration update can be made independently from the contact detection by adding an independent loop detecting the minima and used to update the mean step duration.

Solution	Temporal condition	Weakness
Maxima detection, $f_c = 3$Hz	$\Delta t_{contact} > 0.6 * \frac{2\pi}{\omega}$	Dependency on the starting time
Minima detection	/	Variation of the delay
Maxima detection, $f_c = 3$Hz	$\Delta t_{contact} > 0.7 * d_{step}$	Dependency of the detection condition on the detection

Table 5.1: Summary of the solutions proposed and their weaknesses.

The remaining weakness of this method is its dependency on the starting time of the experiment. Even though one can visually verify that the code is activated close to heel-strike to avoid a wrong departure, it would be more robust to add a condition to maxima detection. A time condition since the last minima detection could for example be added to the conditions of contact detection, with a sufficient margin to overcome its variability.

5.2 Expected results

By updating the C# code with the new detection and vibration conditions, the experiment can be made. As a reminder: during the experiment, the subject walks on a treadmill at a walking speed of 3km/h. One IMU is fixed to his right shank and the shank angular velocity data are analysed in real time to activate the vibration of a vibrotactile unit at heel-strike or after a delay. The vibrotactile unit is fixed to the subject's knee, facing his right patellar tendon. A second IMU is fixed to his left shank to register the gait data of the controlateral side.

The data to analyse after the experiment are thus the gait signals registered by both IMUs. The first analysis to make would be analysing the gait evolution of both legs over time for each condition as well as analysing the symmetry of the gait for each condition. The step duration over time can firstly be analysed visually then statistical tools such as t-tests can be used to assess if the difference between the mean step size at the start and at the the end of the trial is significant or not.

To compare the step duration of both legs for each condition, t-test can also be used. The results obtained in zero-delay condition would give a first clue on the significance of the results for the other two conditions. Indeed, if the difference in mean step duration is already significant in zero-delay condition, the presence of vibrations only, without taking the delay into account, would already have an impact on the results obtained with a delayed vibration. To compare the mean step duration of each leg in the three conditions (zero-delay, positive-delay and negative-delay), one-way ANOVAs can be used to tell us whether the mean step duration depends on the delay factor or not.

The expected results on the right (perturbed) leg are a significantly different mean step duration in the three conditions. By making the hypothesis that the step duration will not be affected by the zero-delay stimulation, we expect the step duration to be longer when a positive delay is added to the stimulation and shorter for a negative delay. Indeed, since the subject will associate the zero-delay stimulation to heel-strike, delaying the stimulation will give him the impression that he touches the ground later. He will therefore lengthen his next step to match the previous sensed step duration. His step duration will probably stabilise with time given that the walking speed is fixed. The left leg step duration is expected to undergo the same changes because the subject will try and keep his gait symmetrical. This evolution could happen with a delay compared to the right leg step duration evolution. All these expected results are, of course, hypothesis to verify with the actual results of the experiment.

Conclusion

The lack of sensory feedback following a lower-limb amputation induces several medical conditions due to an unnatural gait resulting from unsuitable motor commands. Lots of experiments have already been conducted to develop augmented feedback from prostheses, mainly through vibrotactile and electrotactile stimulation. The goal of this thesis was to propose a new gait perturbation experiment to participate in research on sensory feedback for lower-limb prostheses.

After comparison of two potentially stimulated areas (patellar tendon and common fibular nerve) and their respective stimulation modalities (vibrotactile and electrotactile stimulation), the choice was made to provide the perturbation through vibrotactile stimulation of the patellar tendon. The goal was to add information to the proprioceptive feedback of the subject's right leg through this stimulation. The unperturbed condition was defined as a stimulation at heel-strike and the perturbation as the addition of a delay, either positive or negative. To provide the zero-delay stimulation simultaneously to heel-strike, inertial measurement units fixed to the shank were chosen to acquire gait data.

To be able to detect the contact times as precisely as possible, the data received from the IMU had to be treated and analysed in real time. The shank angular velocity signal was chosen for this real-time analysis since it allows an easy identification of gait phases. To decrease the risk of wrong detection, a low-pass filter with cut-off frequency of 5Hz was coded to filter the signal. The signal was then learned by adaptative oscillators to be able to use its fundamental features for contact detection and vibration activation. The contact conditions were defined to detect maxima with a minimum value of 50 deg/s and a minimum temporal delay depending on the fundamental frequency. The software delay induced by the filter and the hardware delay of the vibrotactile device were then computed to be taken into account in the activation of the stimulation. Finally, the conditions of stimulation activation were defined: a phase reset signal was computed to manage the delays and a temporal condition was added between two activations.

Based on the results from the first experiment, several solutions were proposed to improve the contact detection as well as the stimulation activation. The first solution consisted in applying a stronger filter to the signal, with a cut-off frequency of 3Hz. The second possibility was to detect the minima of the signal instead of the maxima. This removed the risk of detecting a wrong event since there is only one minimum per step versus two maxima. The last option was to change the conditions of detection by making them dependent on the step duration instead of the learned frequency. This solution was proposed after observing that the learned frequency was underestimated by the adaptative oscillators. For the first two solutions, the total delay to take into account in the vibration activation was recomputed. The impact of the underestimation of the learned frequency on delay management was then analysed.

The weaknesses of these three solutions were then discussed in order to chose which should be used for contact detection and vibration activation in the final experiment. The dependency of the maxima detection on the starting time of the experiment was highlighted, the variability of the delay between mid-swing and heel-strike for minima detection also, and finally the dependency of

the detection condition on the detection itself for the last solution. From there, the final solution was chosen as a mix of the three propositions. Indeed, it uses a stronger low-pass filter, detects contacts based on conditions on the step duration and uses minima detection to measure the step duration, in order to avoid a dependency between the conditions of contact detection and the detection itself. The remaining weakness of the experimental protocol remains the variation of the hardware delay making the stimulation time imprecise. By translating these conditions in C# and by making the experiment again, the main expected results are a modification of the step duration depending on the stimulation delay with respect to contact time for the perturbed leg and a delayed modification of same amplitude for the unperturbed leg.

To make the current experiment more precise and its results more reliable, another stimulating device with a more constant delay should be considered. A more complete information on the gait kinematic of the subject could also be obtained by adding measuring devices such as cameras detecting markers placed on the subject. This could lead to more precise informations about the effects of the vibrotactile stimulation on the gait of the subject.

Finally, after validation of this experiments on healthy subjects and analysis of the results, an interesting further analysis would be to see if the algorithm is robust for lower walking speeds, closer to the speed of amputees. Once validated, the experiment could be made on amputated subjects to see whether their gait is more symmetrical with a vibrotactile feedback on the amputated limb than without.

Bibliography

[1] Simona Crea, Christian Cipriani, Marco Donati, Maria Chiara Carrozza, and Nicola Vitiello. Providing time-discrete gait information by wearable feedback apparatus for lower-limb amputees : usability and functional validation. *IEEE*, page 8, 2015.

[2] Christian B. Redd and Stacy J. Morris Bamberg. A wireless sensory feedback system for real-time gait modification. *IEEE*, page 5, 2011.

[3] Graham Webb. Providing real-time biofeedback for amputee gait retraining using labview. page 2, 2011.

[4] G. D. Webb, S. Cirovic, S. Ghoussayni, and D. J. Ewins. Electro-tactile sensation thresholds for an amputee gait-retraining system. page 2, 2012.

[5] Ming-Yih Lee, Chih-Feng Lin, and Kok-Soon Soon. Balance control enhancement using sub-sensory stimulation and visual-auditory biofeedback strategies for amputee subjects. *Prosthetics and Orthotics International*, 31(4):342–352, 2007.

[6] Ming-Yih Lee, Chih-Feng Lin, and Kok-Soon Soon. New computer protocol with subsensory stimulation and visual/auditory biofeedback for balance assessment in amputees. *Journal of computers*, 4(10):1005–1011, 2009.

[7] L. Yang, P.S. Dyer, R.J. Carson, J.B. Webster, K. Bo Foreman, and S.J.M. Bamberg. Utilization of a lower extremity ambulatory feedback system to reduce gait asymmetry in transtibial amputation gait. *Elsevier - Gait and Posture*, 36:631–634, 2012.

[8] Aaron Plauché, Dario Villarreal, and Robert D. Gregg. A haptic feedback system for phase-based sensory restoration in above-knee prosthetic leg users. *IEEE Transactions on Haptics*, Y(X):6, 201Z.

[9] Michael R. Tucker, Jeremy Olivier, Anna Pagel, Hannes Bleuler, Mohamed Bouri, Olivier Lambercy, José del R. Millán, Robert Riener, Heike Vallery, and Roger Gassert. Control strategies for active lower extremity prosthetics and orthotics: a review. *Journal of NeuroEngineering and Rehabilitation*, 12(1):29, 2015.

[10] Stacy J. Morris Bamberg, Randy J. Carson, Gregory Stoddard, Philip S. Dyer, and Joseph B. Webster. The lower extremity ambulation feedback system for analysis of gait asymmetries: Preliminary design and validation results. *Journal of Prosthetics and Orthotics*, 22(1):31–36, 2010.

[11] Daniel H. K. Chow and Chris T. K. Cheng. Quantitative analysis of the effects of audio biofeedback on weight-bearing characteristics of persons with transtibial amputation during early prosthetic ambulation. *Journal of Rehabilitation Research and Development*, 37(3):255–260, 2000.

[12] Richard E. Fan, Martin O. Culjat, Chih-Hung King, Miguel L. Franco, Richard Boryk, James W. Bisley, Erik Dutson, and Warren S. Grundfest. A haptic feedback system for lower-limb prostheses. *IEEE Transactions on Neural Systems and Rehabilitation Engineering*, 16(3):270–277, 2008.

[13] Julie Duqué. LIEPR1024 - Fondements neuro-physiologiques et neuro-psychologiques de l'apprentissage et du controle moteur, 2015. Course at Université Catholique de Louvain.

[14] Streifeneder. The eight phases of human gait cycle. `https://www.streifeneder.com/downloads/o.p./400w43_e_poster_gangphasen_druck.pdf`. [Online; accessed 23-January-2018].

[15] Daniela Zambarbieri, Micaela Schmid, and Gennaro Verni. *Intelligent Systems and Technologies in Rehabilitation Engineering*, chapter Sensory feedback for lower limb prostheses, page 24. CRC Press LLC, 2001.

[16] J. Miles Canino and Kevin B. Fite. The effects of cutaneous haptic feedback on emg-based motion control of a transfemoral prosthesis. page 8, 2016.

[17] Calogero Maria Oddo, Stanisa Raspopovic, Fiorenzo Artoni, Alberto Mazzoni, Giacomo Spigler, Francesco Petrini, Federica Giambattistelli, Fabrizio Vecchio, Francesca Miraglia, Loredana Zollo, Giovanni Di Pino, Domenico Camboni, Maria Chiara Carrozza, Eugenio Guglielmelli, Paolo Maria Rossini, Ugo Faraguna, and Silvestro Micera. Intraneural stimulation elicits discrimination of textural features by artificial fingertip in intact and amputee humans. *eLife*, page 27, 2016.

[18] C. Antfolk, M. D'Alonzo, B. Rosén, G. Lundborg, F. Sebelius, and C. Cipriani. Sensory feedback in upper limb prosthetics. *Expert Reviews of Medical Devices*, page 22, 2013.

[19] Enzo Mastinu. Embedded controller for artificial limbs. page 94, 2017.

[20] Dorindo G. Buma, Jan R. Buitenweg, and Peter H. Veltink. Intermittent stimulation delays adaptation to electrocutaneous sensory feedback. *IEEE Transactions on Neural Systems and Rehabilitation Engineering*, 15(3):435–441, 2007.

[21] J. Miles Canino and Kevin B. Fite. Haptic feedback in lower-limb prosthesis - combined haptic feedback and emg control of a powered prosthesis. *IEEE*, page 4, 2016.

[22] Marco D'Alonzo, Strahinja Dosen, Christian Cipriani, and Dario Farina. Hyve: Hybrid vibro-electrotactile stimulation for sensory feedback and substitution in rehabilitation. *IEEE Transactions on Neural Systems and Rehabilitation Engineering*, page 12, 2013.

[23] Marco D'Alonzo, Strahinja Dosen, Christian Cipriani, and Dario Farina. Hyve – hybrid vibro-electrotactile stimulation – is an efficient approach to multi-channel sensory feedback. *IEEE*, page 10, 2014.

[24] Strahinja Dosen, Marko Markovic, Kelef Somer, Bernhard Graimann, and Dario Farina. Emg biofeedback for online predictive control of grasping force in a myoelectric prosthesis. *Journal of NeuroEngineering and Rehabilitation*, page 13, 2015.

[25] Strahinja Dosen, Marko Markovic, Matija Strbac, Minja Belic, Vladimir Kojic, Goran Bijelic, Thierry Keller, and Dario Farina. Multichannel electrotactile feedback with spatial and mixed coding for closed-loop control of grasping force in hand prostheses. *IEEE Transactions on Neural Systems and Rehabilitation Engineering*, 25(3):183–195, 2017.

[26] Nikola Jorgovanovic, Strahinja Dosen, Damir J. Djozic, Goran Krajoski, and Dario Farina. Virtual grasping: Closed-loop force control using electrotactile feedback. *Computational and Mathematical Methods in Medicine*, page 13, 2014.

[27] Max Ortiz-Catalan, Bo Håkansson, and Rickard Brånemark. An osseointegrated human-machine gateway for long-term sensory feedback and motor control of artificial limbs. *Science Translational Medicine*, 6(257):8, 2014.

[28] S. Raspopovic, M. Capogrosso, F. Petrini, M. Bonizzato, J. Rigosa, G. Di Pino, J. Carpaneto, M. Controzzi, T. Boretius, E. Fernandez, G. Granata, C. M. Oddo, L. Citi, A.L. Ciancio, C. Cipriani, M.C. Carrozza, W. Jensen, E. Guglielmelli, T. Stieglitz, P.M. Rossini, and S. Micera. Restoring natural sensory feedback in real-time bidirectional hand prostheses. *Science Translational Medicine*, 6(222):20, 2015.

[29] Suzanne Wendelken, David M. Page, Tyler Davis, Heather A. C. Wark, David T. Kluger, Christopher Duncan, David J. Warren, Douglas T. Hutchinson, and Gregory A. Clark. Restoration of motor control and proprioceptive and cutaneous sensation in humans with prior upper-limb amputation via multiple utah slanted electrode arrays (useas) implanted in residual peripheral arm nerves. *Journal of NeuroEngineering and Rehabilitation*, 14(121):17, 2017.

[30] E.C. Wentink, A. Mulder, J.S. Rietman, and P.H. Veltink. Vibrotactile stimulation of the upper leg: Effects of location, stimulation method and habituation. *IEEE*, page 4, 2011.

[31] Kenhub. Patellar tendon. `https://www.kenhub.com/en/library/anatomy/patellar-tendon`. [Online; accessed 07-April-2018].

[32] Kenhub. Quadriceps femoris muscle. `https://www.kenhub.com/en/library/anatomy/the-quadriceps-femoris-muscle`. [Online; accessed 07-April-2018].

[33] Haluk Çabuk and Fatmagül Kuşku Çabuk. Mechanoreceptors of the ligaments and tendons around the knee. *Clinical Anatomy*, 29:789–795, 2016.

[34] Emmanuele Tidoni, Gabriele Fusco, Daniele Leonardis, Antonio Frisoli, Massimo Bergamasco, and Salvatore Maria Aglioti. Illusory movements induced by tendon vibration in right- and left-handed people. *Experimental Brain Research*, 233:375–383, 2015.

[35] Edith Ribot-Ciscar, Mikael Bergenheim, Frédéric Albert, and Jean-Pierre Roll. Proprioceptive population coding of limb position in humans. *Experimental Brain Research*, 149:512–519, 2003.

[36] Sarah Calvin-Figuière, Patricia Romaiguère, Jean-Claude Gilhodes, and Jean-Pierre Roll. Antagonist motor responses correlate with kinesthetic illusions induced by tendon vibration. *Experimental Brain Research*, 124:342–350, 1999.

[37] Sarah Calvin-Figuière, Patricia Romaiguère, and Jean-Pierre Roll. Relations between the directions of vibration-induced kinesthetic illusions and the pattern of activation of antagonist muscles. *Brain Research*, 881:128–138, 2000.

[38] Frederic Albert, Mikael Bergenheim, Edith Ribot-Ciscar, and Jean-Pierre Roll. The ia afferent feedback of a given movement evokes the illusion of the same movement when returned to the subject via muscle tendon vibration. *Experimental Brain Research*, 172:163–174, 2006.

[39] Grégoire Courtine, Alessandro Marco De Nunzio, Micaela Schmid, Maria Vittoria Beretta, and Marco Schieppati. Stance- and locomotion-dependent processing of vibration-induced

proprioceptive inflow from multiple muscles in humans. *Journal of Neurophysiology*, 97:772–779, 2007.

[40] Jean-Pierre Roll, Frédéric Albert, Chloé Thyrion, Edith Ribot-Ciscar, Mikael Bergenheim, and Benjamin Mattei. Inducing any virtual two-dimensional movement in humans by applying muscle tendon vibration. *Journal of Neurophysiology*, 101:816–823, 2009.

[41] Kenhub. Common fibular nerve. `https://www.kenhub.com/en/library/anatomy/common-fibular-nerve`. [Online; accessed 07-April-2018].

[42] Kenhub. Common peroneal nerve. `https://www.kenhub.com/en/library/anatomy/common-peroneal-nerve`. [Online; accessed 07-April-2018].

[43] Kenhub. Nervus peroneus superficialis. `https://www.kenhub.com/en/atlas/nervus-peroneus-superficialis`. [Online; accessed 10-April-2018].

[44] Kenhub. The anterior muscles of the lower leg. `https://www.kenhub.com/en/library/anatomy/anterior-muscles-of-the-lower-leg`. [Online; accessed 10-April-2018].

[45] Kenhub. Musculus extensor digitorum brevis. `https://www.kenhub.com/en/atlas/extensor-digitorum-brevis-muscle`. [Online; accessed 10-April-2018].

[46] Kenhub. Musculus extensor hallucis brevis. `https://www.kenhub.com/de/atlas/extensor-hallucis-brevis-muscle`. [Online; accessed 10-April-2018].

[47] Michael E. Knash, Aiko Kido, Monica Gorassini, K. Ming Chan, and Richard B. Stein. Electrical stimulation of the human common peroneal nerve elicits lasting facilitation of cortical motor-evoked potentials. *Experimental Brain Research*, 153:366–377, 2003.

[48] Tactile Labs. Haptuator original. `http://tactilelabs.com/products/haptics/haptuator/`. [Online; accessed 17-May-2018].

[49] Hsin-Yun Yao and Vincent Hayward. Design and analysis of a recoil-type vibrotactile transducer. *Acoustical Society of America*, 128(2):619–627, 2010.

[50] Simona Crea, Benoni B. Edin, Kristel Knaepen, Romain Meeusen, and Nicola Vitiello. Time-discrete vibrotactile feedback contributes to improved gait symmetry in patients with lower limb amputations: Case series. *Physical Therapy*, 97(2):198–207, 2017.

[51] x IO Technologies. Open source imu and ahrs algorithms. `http://x-io.co.uk/open-source-imu-and-ahrs-algorithms/`. [Online; accessed 08-May-2018].

[52] x-io Technologies. x-imu. `http://x-io.co.uk/x-imu/`. [Online; accessed 08-August-2018].

[53] Barry R. Greene, Denise McGrath, Ross O'Neill, Karol O'Donovan, Adrian Burns, and Brian Caulfield. An adaptive gyroscope-based algorithm for temporal gait analysis. *Medical & Biological Engineering & Computing*, 48:1251–1260, 2010.

[54] Jan M. Jasiewicz, John H.J. Allum, James W. Middleton, Andrew Barriskill, Peter Condie, Brendan Purcell, and Raymond Che Tin Li. Gait event detection using linear accelerometers or angular velocity transducers in able-bodied and spinal-cord injured individuals. *Gait & Posture*, 24:502–509, 2006.

[55] Darwin Gouwanda and Alpha Agape Gopalai. A robust real-time gait event detection using wireless gyroscope and its application on normal and altered gaits. *Medical Engineering and Physics*, 37:219–225, 2015.

[56] Soo Chan Kim, Joo Yeon Kim, Hwan Nyeong Lee, Hwan Ho Lee, Jae Hwan Kwon, Nam beom Kim, Mi Joo Kim, Jong Hyun Hwang, and Gyu Cheol Han. A quantitative analysis of gait patterns in vestibular neuritis patients using gyroscope sensor and a continuous walking protocol. *Journal of NeuroEngineering and Rehabilitation*, 11(58):9, 2014.

[57] E. Allseits, J. Lučarević, R. Gailey, V. Agrawal, I. Gaunaurd, and C. Bennett. The development and concurrent validity of a real-time algorithm for temporal gait analysis using inertial measurement units. *Journal of Biomechanics*, 55:27–33, 2017.

[58] Denise McGrath, Barry R. Greene, Karol J. O'Donovan, and Brian Caulfield. The development and concurrent validity of a real-time algorithm for temporal gait analysis using inertial measurement units. *Sports Engineering*, 15:207–2013, 2012.

[59] Tingfang Yan, Andrea Parri, Virginia Ruiz Garate, Marco Cempini, Renaud Ronsse, and Nicola Vitiello. An oscillator-based smooth real-time estimate of gait phase for wearable robotics. *Auton Robot*, 41:759–774, 2017.

List of Figures

List of Tables

Appendix A

Choice of the signal

Signals registered by the IMU, corresponding to the accelerations along the 3 axis and the angular velocities around the x- and y-axis.

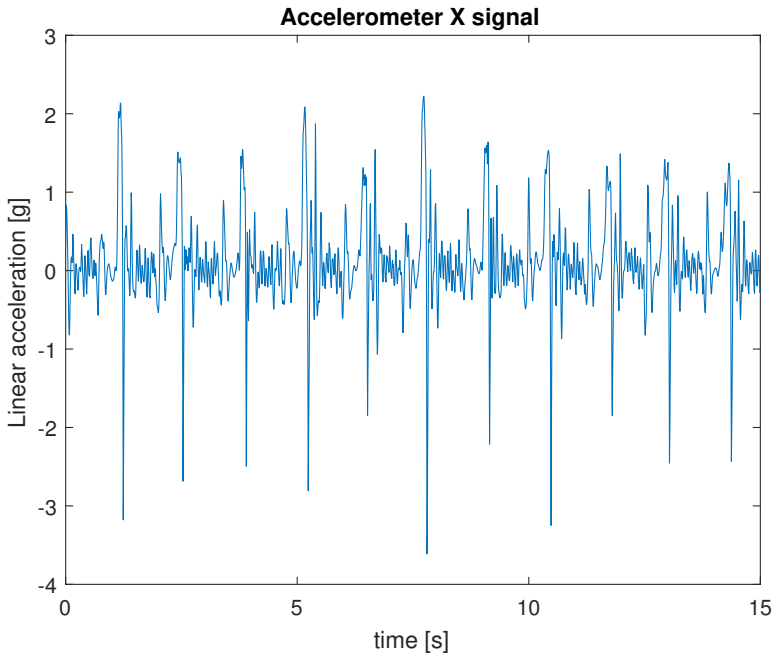

Figure A.1: Accelerometer signal along the x-axis.

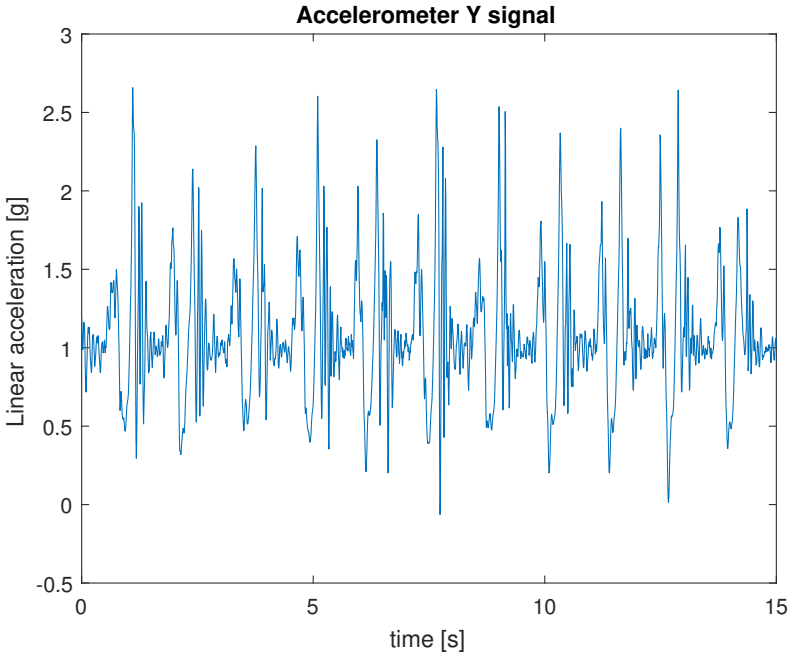

Figure A.2: Accelerometer signal along the y-axis.

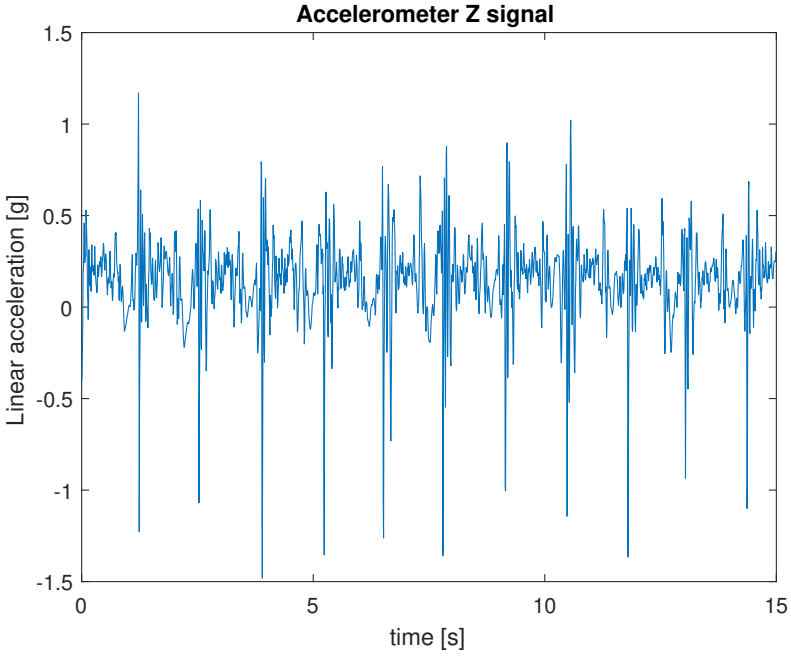

Figure A.3: Accelerometer signal along the z-axis.

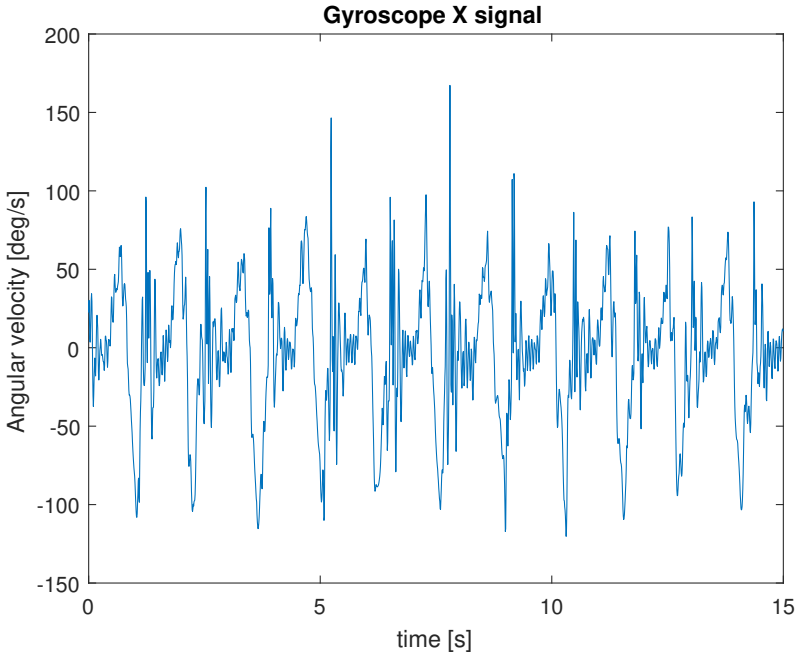

Figure A.4: Gyroscopic signal around the x-axis.

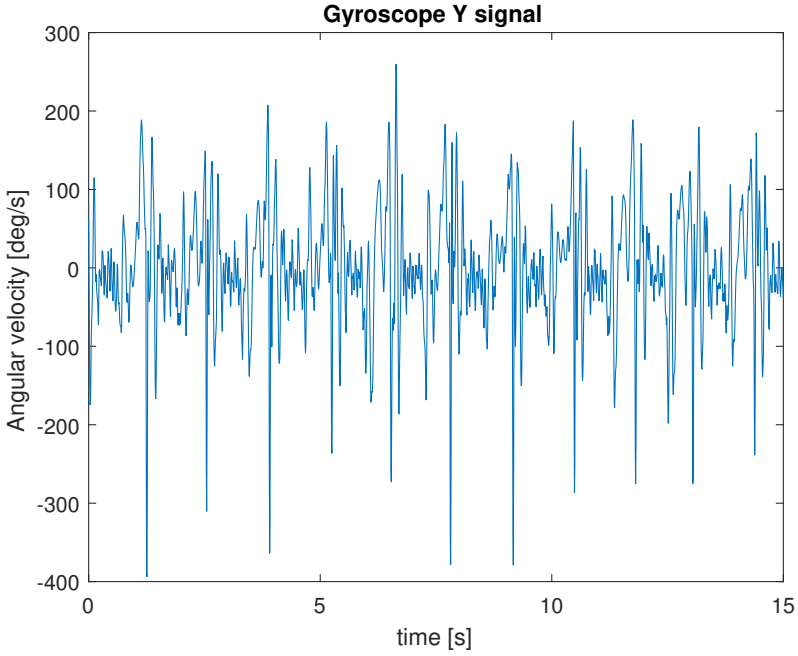

Figure A.5: Gyroscopic signal around the y-axis.

Appendix B

ρ value determination

Contact detection on the shank angular velocity signal by changing the ρ parameter of the temporal condition $\Delta t_{contact} > \rho * \frac{2\pi}{\omega}$.

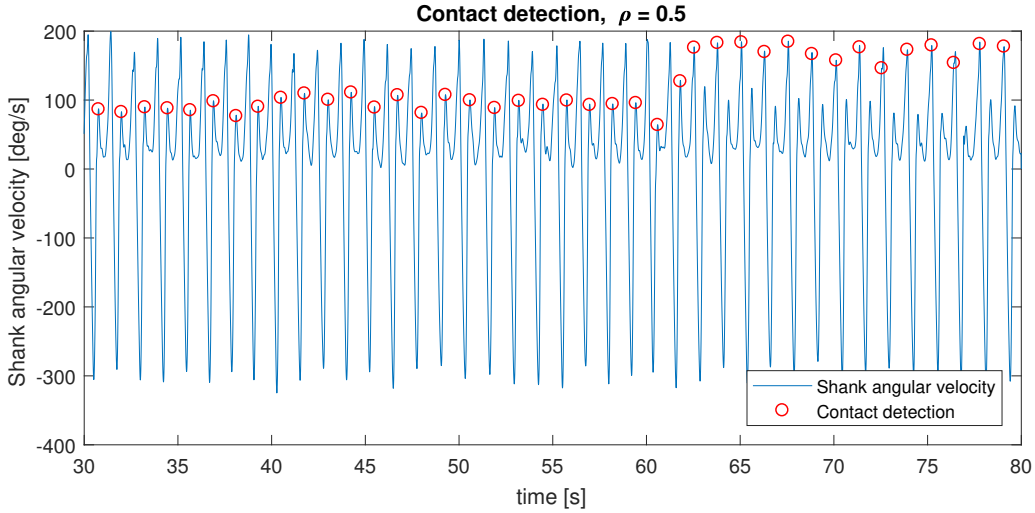

Figure B.1: Contact detection with $\rho = 0.5$.

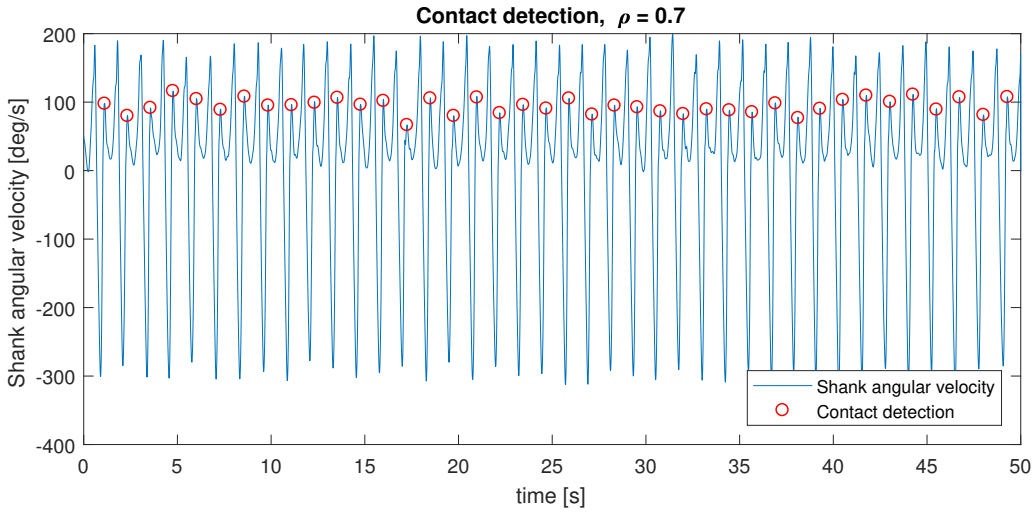

Figure B.2: Contact detection with $\rho = 0.7$.

Appendix C

Contact detection at different velocities

Contact detection on the shank angular velocity signal filtered with a cut-off frequency of 3Hz for walking speeds of 4km/h and 5km/h. The parameter ρ of the contact detection condition

$$\Delta t_{contact} > \rho * \frac{2\pi}{\omega}$$

is fixed to 0.7.

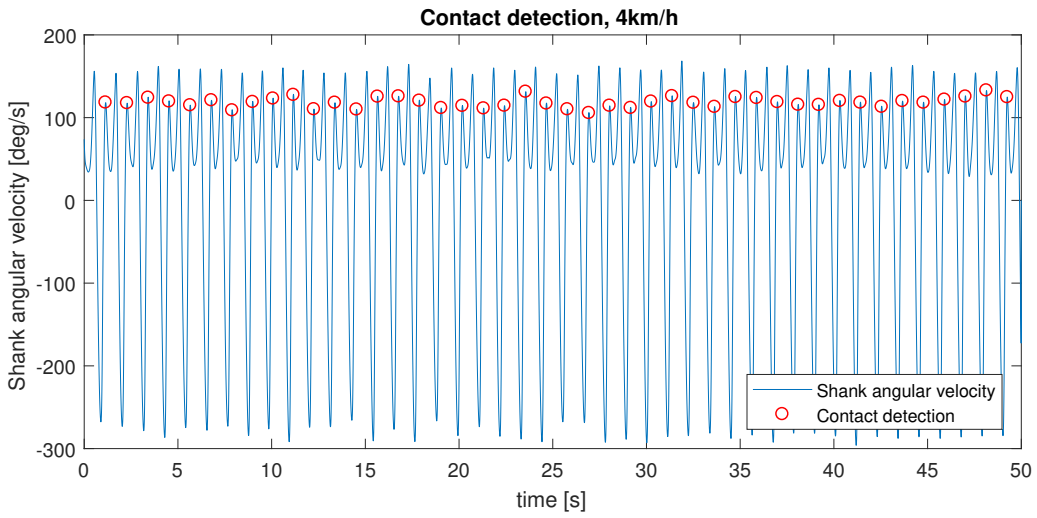

Figure C.1: Contact detection at 4km/h with $f_c = 3$Hz and $\rho = 0.7$.

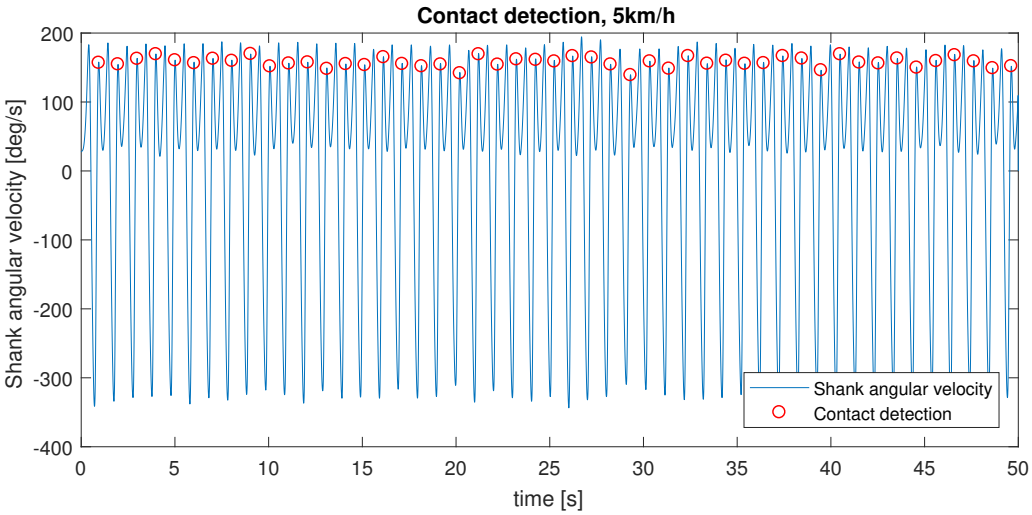

Figure C.2: Contact detection at 5km/h with $f_c = 3$Hz and $\rho = 0.7$.

Rue Archimède, 1 bte L6.11.01, 1348 Louvain-la-Neuve **www.uclouvain.be/epl**